Universität Karlsruhe (TH)
Institut für Baustatik

A robust nonlinear mixed hybrid quadrilateral shell element

W. Wagner, F. Gruttmann

Mitteilung 3(2004)

Universität Karlsruhe (TH)
Institut für Baustatik

A robust nonlinear mixed hybrid quadrilateral shell element

W. Wagner, F. Gruttmann

Mitteilung 3(2004)

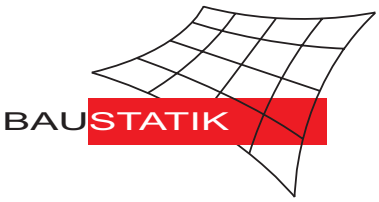

Prof. Dr.–Ing. W. Wagner
Institut für Baustatik
Universität Karlsruhe
Postfach 6980
76128 Karlsruhe

Telefon: (0721) 608–2280
Telefax: (0721) 608–6015
E–mail: bs@.uni-karlsruhe.de
Internet: http://www.bs.uni-karlsruhe.de

A robust nonlinear mixed hybrid quadrilateral shell element

W. Wagner

Institut für Baustatik
Universität Karlsruhe (TH)
Kaiserstraße 12
76131 Karlsruhe
Germany

F. Gruttmann

Institut für Werkstoffe und Mechanik im Bauwesen
Technische Universität Darmstadt
Petersenstraße 12
64287 Darmstadt
Germany

Contents

Summary In the paper a nonlinear quadrilateral shell element for the analysis of thin structures is presented. The variational formulation is based on a Hu–Washizu functional with independent displacement, stress and strain fields. The interpolation matrices for the mid–surface displacements and rotations as well as for the stress resultants and strains are specified. Restrictions on the interpolation functions concerning fulfilment of the patch test and stability are derived. The developed mixed hybrid shell element possesses the correct rank and fulfills the in–plane and bending patch test. Using Newton´s method the finite element approximation of the stationary condition is iteratively solved. Our formulation can accommodate arbitrary nonlinear material models for finite deformations. In the examples we present results for isotropic plasticity at finite rotations and small strains as well as bifurcation problems and post–buckling response. The essential feature of the new element is the robustness in the equilibrium iterations. It allows very large load steps in comparison to other element formulations.

Key words: Reissner–Mindlin shell theory, Hu–Washizu variational principle, quadrilateral shell element, shell intersections, large load steps

1 Introduction

Computational shell analysis is based on a stress resultant theory e.g. [1, 2] or on the so–called degenerated approach [3]. Although the hypotheses underlying the classical shell theory and degenerated approach are essentially the same, the reduction to resultant form is typically carried out analytically in the former, and numerically in the latter, [4]. Many of the computational shell models consider transverse shear deformations within a Reissner–Mindlin theory [5], [6] to by–pass the difficulties caused by C^1–requirements of the Kirchhoff–Love theory, see e.g. [7, 8, 9].

Generally, shell behaviour is extremely sensitive to initial geometry and imperfections, thus a successful correlation between theory and analysis is achieved only after including specific details of these quantities. Low order elements like quadrilaterals based on standard displacement interpolation are usually characterized by locking phenomena. In shells two types of locking occur: transverse shear locking in which bending modes are excluded and nearly all energy is stored in transverse shear terms, and membrane locking in which all bending energy is restrained and energy is stored in membrane terms. Elements which exhibit a locking tendency lead to unacceptable stiff results when reasonable finite element meshes are employed.

In attempting to avoid locking, reduced integration methods have been advocated, see e.g. [10]. Use of reduced (or selective reduced) integration is often accompanied by spurious zero energy modes. Hence, authors have developed stabilization techniques to regain the correct rank of the element stiffness matrix, e.g. [7, 11, 12, 13]. In some cases, however, results turned out to be sensitive to the ad hoc hourglass control parameters. In Ref. [14] a so-called physical stabilization matrix is derived from the orthogonality between the constant part of

the strain field and the non-constant part.
Mixed variational principles provide the basis for the discussed finite element techniques. Assuming linear elasticity a Hellinger–Reissner functional has been used in e.g. [9]. For general nonlinear material behaviour a three field variational functional with independent displacements, stresses and strains is more appropriate. Within the so–called enhanced strain formulations the independent stresses are eliminated from the set of equations using orthogonality conditions and a two field formulation remains, [15]. For shells this method has been applied enhancing the Green–Lagrangean membrane strains e.g. in [16, 17]. The corresponding developments for so–called solid shell elements have been presented in e.g. [18, 19]
A further new development on enhanced strain formulations is based on a modified Hu–Washizu formulation, [20]. The functional for plane elasticity problems contains displacements, stresses, strains and enhanced strains as independent variables. An effective method to avoid transverse shear locking is based on assumed shear strain fields first proposed in [21], and subsequently extended in [22, 23, 24]. The variational basis for these methods is the Hu–Washizu functional.
An important issue within the context of developing a finite shell model is the number and type of rotational parameters on the element. Mostly general shell theories exclude explicit dependence of a rotational field about the normal to the shell surface which leads to a five parameter model (three displacements and two local rotations). Use of 5 degree–of–freedom frame requires construction of special coordinate systems for the rotational parameters. Considering the so–called drilling degree-of–freedom leads to a finite element discretization with six nodal parameters. This has some advantages since both displacement and rotation parameters are associated with a global coordinate frame. On the other hand a larger set of algebraic equations has to be solved, e.g. [25].

The new aspects and essential features of the present formulation are summarized as follows:

(i) The kinematics of the shell for finite deformations including transverse shear strains is formulated assuming an inextensible director field. The nonlinear variational formulation is based on a Hu–Washizu functional using a material representation with independent displacements, stresses and strains. The consideration of arbitrary nonlinear constitutive models is possible. As an example we implement isotropic plasticity with hardening for small strains. Due to the inextensibility of the current director vector the plane stress condition has to be enforced.

(ii) Convergence and stability conditions on the construction of interpolation functions for the independent stress resultants and strains are investigated. As result the derived mixed hybrid quadrilateral element fulfills the membrane patch test and bending patch test and possesses the correct rank. Partly the element matrices are integrated analytically which leads to a fast and effective stiffness computation.

(iii) We test the element formulation within several nonlinear examples including inelastic material behaviour and stability problems. The results are compared with those obtained with four–noded enhanced strain elements (EAS-shell [17]). Especially for large load steps the new element needs essentially less iterations compared with the EAS–elements.

(iv) The element formulation allows the analysis of shells with intersections. The nodal degrees of freedom are: three global displacements components, three global rotations at nodes on intersections or two local rotations at other nodes.

2 Kinematics and Variational Formulation

To introduce our notation we briefly outline the basic equations of the Reissner–Mindlin shell model. Furthermore the three-field variational principle is formulated in this section.
Let $\mathcal{B}$ be the three–dimensional Euclidean space occupied by the shell in the reference configuration. The position vector $\mathbf{\Phi}$ of any point $P \in \mathcal{B}_0$ is defined by

$$\begin{aligned} &\mathbf{\Phi}(\xi^1,\xi^2,\xi^3) = \Phi^i\,\mathbf{e}_i = \mathbf{X} + \xi^3\,\mathbf{D}(\xi^1,\xi^2) \\ &\text{with} \quad |\mathbf{D}(\xi^1,\xi^2)| = 1 \quad \text{and} \quad -\frac{h}{2} \le \xi^3 \le \frac{h}{2} \end{aligned} \tag{1}$$

where $\mathbf{X}(\xi^1,\xi^2)$ denotes the position vector of the shell mid–surface Ω. With ξ^i and $\mathbf{e}_i$ we denote a convected coordinate system of the body and the global cartesian basis system, respectively. A director $\mathbf{D}(\xi^1,\xi^2)$ is defined as a vector perpendicular to the shell mid–surface. The usual summation convention is used, where Latin indices range from 1 to 3 and Greek indices range from 1 to 2. Hence, the geometry of the deformed shell space $\mathcal{B}$ is described by

$$\boldsymbol{\phi}(\xi^1,\xi^2,\xi^3) = \phi^i\,\mathbf{e}_i = \mathbf{x}(\xi^1,\xi^2) + \xi^3\,\mathbf{d}(\xi^1,\xi^2) \qquad \text{with} \quad |\mathbf{d}(\xi^1,\xi^2)| = 1\,. \tag{2}$$

The inextensible director $\mathbf{d}$ is obtained using an orthogonal tensor $\mathbf{R}$ and the initial vector $\mathbf{D}$. Since $\mathbf{d}$ is not normal to the current configuration the kinematic assumption (2) allows for transverse shear strains. In a standard way the deformation gradient reads $\mathbf{F} = \operatorname{Grad}\boldsymbol{\phi}$ and the Green–Lagrangean strain tensor with covariant components E_{ij} and contravariant basis $\mathbf{G}^i$ is given

$$\mathbf{E} = \frac{1}{2}(\mathbf{F}^T\mathbf{F} - \mathbf{1}) = E_{ij}\,\mathbf{G}^i \otimes \mathbf{G}^j\,, \qquad E_{ij} = \frac{1}{2}(\boldsymbol{\phi}_{,i}\cdot\boldsymbol{\phi}_{,j} - \mathbf{\Phi}_{,i}\cdot\mathbf{\Phi}_{,j})\,. \tag{3}$$

Here, commas denote partial differentiation with respect to the coordinates ξ^i. Inserting the equations (1) and (2) in $(3)_2$ yields

$$\begin{aligned} E_{\alpha\beta} &= \varepsilon_{\alpha\beta} + \xi^3\,\kappa_{\alpha\beta} + (\xi^3)^2\,\rho_{\alpha\beta} \\ 2\,E_{\alpha 3} &= \gamma_\alpha \\ E_{33} &= 0 \end{aligned} \tag{4}$$

with the shell strains

$$\begin{aligned} \varepsilon_{\alpha\beta} &= \frac{1}{2}(\mathbf{x}_{,\alpha}\cdot\mathbf{x}_{,\beta} - \mathbf{X}_{,\alpha}\cdot\mathbf{X}_{,\beta}) \\ \kappa_{\alpha\beta} &= \frac{1}{2}(\mathbf{x}_{,\alpha}\cdot\mathbf{d}_{,\beta} + \mathbf{x}_{,\beta}\cdot\mathbf{d}_{,\alpha} - \mathbf{X}_{,\alpha}\cdot\mathbf{D}_{,\beta} - \mathbf{X}_{,\beta}\cdot\mathbf{D}_{,\alpha}) \\ \gamma_\alpha &= \mathbf{x}_{,\alpha}\cdot\mathbf{d} - \mathbf{X}_{,\alpha}\cdot\mathbf{D} \end{aligned} \tag{5}$$

with membrane strains $\varepsilon_{\alpha\beta}$, curvatures $\kappa_{\alpha\beta}$ and shear strains γ_α. The second order curvatures $\rho_{\alpha\beta}$ are neglected for thin structures. We organize the shell strains in a vector

$$\boldsymbol{\varepsilon}_G = [\varepsilon_{11}, \varepsilon_{22}, 2\varepsilon_{12}, \kappa_{11}, \kappa_{22}, 2\kappa_{12}, \gamma_1, \gamma_2]^T, \tag{6}$$

where the subscript G refers to the Green–Lagrangean strain tensor (3). The work conjugate stress resultants are integrals of the Second Piola–Kirchhoff stress tensor and read

$$\boldsymbol{\sigma} = [n^{11}, n^{22}, n^{12}, m^{11}, m^{22}, m^{12}, q^1, q^2]^T \tag{7}$$

with membrane forces $n^{\alpha\beta} = n^{\beta\alpha}$, bending moments $m^{\alpha\beta} = m^{\beta\alpha}$ and shear forces q^α.

The shell is loaded statically by surface loads $\bar{\mathbf{p}}$ on Ω and by boundary loads $\bar{\mathbf{t}}$ on the boundary Γ_σ. Hence the basic Hu–Washizu functional is formulated in matrix notation

$$\Pi(\mathbf{v}, \boldsymbol{\sigma}, \boldsymbol{\varepsilon}) = \int_{(\Omega)} [W(\boldsymbol{\varepsilon}) + \boldsymbol{\sigma}^T(\boldsymbol{\varepsilon}_G(\mathbf{v}) - \boldsymbol{\varepsilon})]\, dA - \int_{(\Omega)} \mathbf{u}^T \bar{\mathbf{p}}\, dA - \int_{(\Gamma_\sigma)} \mathbf{u}^T\, \bar{\mathbf{t}}\, ds \quad \rightarrow \quad \text{stat.} \tag{8}$$

with the area element of the shell $dA = j\, d\xi^1\, d\xi^2$. Here, $\mathbf{v} = [\mathbf{u}, \boldsymbol{\omega}]^T$, $\boldsymbol{\varepsilon}$, and $\boldsymbol{\sigma}$ denote the independent displacement, strain and stress fields, with $\mathbf{u} = \mathbf{x} - \mathbf{X}$ the displacement vector and $\boldsymbol{\omega}$ the vector of rotational parameters of the shell middle surface. The strain energy W may be an arbitrary function of the independent strains. Introducing $\boldsymbol{\theta} := [\mathbf{v}, \boldsymbol{\sigma}, \boldsymbol{\varepsilon}]^T$ and $\delta\boldsymbol{\theta} := [\delta\mathbf{v}, \delta\boldsymbol{\sigma}, \delta\boldsymbol{\varepsilon}]^T$ the stationary condition reads

$$\begin{aligned} \delta\Pi \;:=\; g(\boldsymbol{\theta}, \delta\boldsymbol{\theta}) = &\int_{(\Omega)} [\delta\boldsymbol{\varepsilon}^T(\partial_{\boldsymbol{\varepsilon}} W - \boldsymbol{\sigma}) + \delta\boldsymbol{\sigma}^T(\boldsymbol{\varepsilon}_G - \boldsymbol{\varepsilon}) + \delta\boldsymbol{\varepsilon}_G^T\boldsymbol{\sigma}]\, dA \\ &- \int_{(\Omega)} \delta\mathbf{u}^T \bar{\mathbf{p}}\, dA - \int_{(\Gamma_\sigma)} \delta\mathbf{u}^T\, \bar{\mathbf{t}}\, ds = 0 \end{aligned} \tag{9}$$

with the virtual shell strains $\delta\boldsymbol{\varepsilon}_G = [\delta\varepsilon_{11}, \delta\varepsilon_{22}, 2\delta\varepsilon_{12}, \delta\kappa_{11}, \delta\kappa_{22}, 2\delta\kappa_{12}, \delta\gamma_1, \delta\gamma_2]^T$

$$\begin{aligned} \delta\varepsilon_{\alpha\beta} &= \frac{1}{2}(\delta\mathbf{x}_{,\alpha} \cdot \mathbf{x}_{,\beta} + \delta\mathbf{x}_{,\beta} \cdot \mathbf{x}_{,\alpha}) \\ \delta\kappa_{\alpha\beta} &= \frac{1}{2}(\delta\mathbf{x}_{,\alpha} \cdot \mathbf{d}_{,\beta} + \delta\mathbf{x}_{,\beta} \cdot \mathbf{d}_{,\alpha} + \delta\mathbf{d}_{,\alpha} \cdot \mathbf{x}_{,\beta} + \delta\mathbf{d}_{,\beta} \cdot \mathbf{x}_{,\alpha}) \\ \delta\gamma_\alpha &= \delta\mathbf{x}_{,\alpha} \cdot \mathbf{d} + \delta\mathbf{d} \cdot \mathbf{x}_{,\alpha}\ . \end{aligned} \tag{10}$$

With integration by parts and applying standard arguments of variational calculus one obtains the associated Euler–Lagrange equations

$$\left.\begin{aligned} \tfrac{1}{j}(j\,\mathbf{n}^\alpha)_{,\alpha} + \bar{\mathbf{p}} &= \mathbf{0} & \qquad \boldsymbol{\varepsilon}_G - \boldsymbol{\varepsilon} &= \mathbf{0} \\ \tfrac{1}{j}(j\,\mathbf{m}^\alpha)_{,\alpha} + \mathbf{x}_{,\alpha} \times \mathbf{n}_\alpha &= \mathbf{0} & \qquad \partial_{\boldsymbol{\varepsilon}} W - \boldsymbol{\sigma} &= \mathbf{0} \end{aligned}\right\} \quad \text{in } \Omega \tag{11}$$

with $\mathbf{n}^\alpha := n^{\alpha\beta}\,\mathbf{x}_{,\beta} + q^\alpha \mathbf{d} + m^{\alpha\beta}\,\mathbf{d}_{,\beta}$ and $\mathbf{m}^\alpha := \mathbf{d} \times m^{\alpha\beta}\,\mathbf{x}_{,\beta}$, where the summation convention for repeated indices is used. The principle yields the static field equations with local form of linear and angular momentum, the geometric field equations and the constitutive law. Furthermore the static boundary conditions $\mathbf{t} - \bar{\mathbf{t}} = \mathbf{0}$ on Γ_σ with $\mathbf{t}$ the boundary forces related to $\mathbf{n}^\alpha$ follow. The geometric boundary conditions $\mathbf{u} - \bar{\mathbf{u}} = \mathbf{0}$ on Γ_u have to be fulfilled as constraints.

3 Finite Element Equations

3.1 Interpolation of the initial and current reference surface

In this section the finite element equations for quadrilaterals are specified applying the isoparametric concept. The local numbering of the corner nodes and midside node can be seen in Fig. 1.

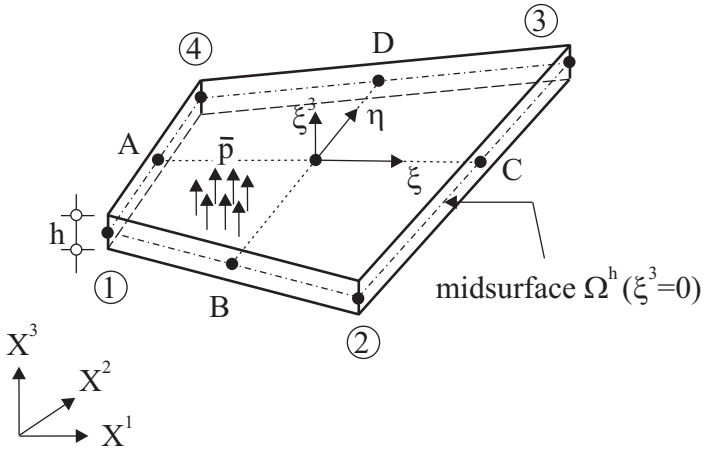

Figure 1: Quadrilateral shell element

A map of the coordinates $\{\xi, \eta\} \in [-1, 1]$ from the unit square to the midsurface in the initial and current configuration is applied. Thus the position vector and the director vector of the reference surface are interpolated with bi–linear functions

$$\mathbf{X}^h = \sum_{I=1}^{4} N_I \, \mathbf{X}_I \qquad \mathbf{D}^h = \sum_{I=1}^{4} N_I \, \mathbf{D}_I \qquad N_I = \frac{1}{4}(1 + \xi_I \xi)(1 + \eta_I \eta) \tag{12}$$

with $\xi_I \in \{-1, \ \ 1, \ \ 1, -1\}$ and $\eta_I \in \{-1, -1, \ \ 1, \ \ 1\}$. The superscript h denotes the characteristic size of the element discretization and indicates the finite element approximation. The nodal position vectors $\mathbf{X}_I$ and local cartesian basis systems $[\mathbf{A}_{1I}, \mathbf{A}_{2I}, \mathbf{A}_{3I}]$ are generated within the mesh input. Here, $\mathbf{D}_I = \mathbf{A}_{3I}$ is perpendicular to Ω and $\mathbf{A}_{1I}$, $\mathbf{A}_{2I}$ are constructed in such a way that the boundary conditions can be accommodated. With $(12)_2$ the orthogonality is only given at the nodes.
For each element a local cartesian basis $\mathbf{t}_i$ is evaluated

$$\begin{aligned}
\bar{\mathbf{d}}_1 &= \mathbf{X}_3 - \mathbf{X}_1 & \hat{\mathbf{d}}_1 &= \bar{\mathbf{d}}_1 / |\bar{\mathbf{d}}_1| \\
\bar{\mathbf{d}}_2 &= \mathbf{X}_2 - \mathbf{X}_4 & \hat{\mathbf{d}}_2 &= \bar{\mathbf{d}}_2 / |\bar{\mathbf{d}}_2| \\
\mathbf{t}_1 &= (\hat{\mathbf{d}}_1 + \hat{\mathbf{d}}_2) / |\hat{\mathbf{d}}_1 + \hat{\mathbf{d}}_2| \\
\mathbf{t}_2 &= (\hat{\mathbf{d}}_1 - \hat{\mathbf{d}}_2) / |\hat{\mathbf{d}}_1 - \hat{\mathbf{d}}_2| \\
\mathbf{t}_3 &= \mathbf{t}_1 \times \mathbf{t}_2 \, .
\end{aligned} \tag{13}$$

One could also use the so-called lamina basis according to [26] where the base vectors $\mathbf{t}_\alpha$ lie

as close as possible to the coordinates ξ and η. Hence the Jacobian matrix $\mathbf{J}$ is defined

$$\mathbf{J} = \begin{bmatrix} \mathbf{X}^h_{,\xi} \cdot \mathbf{t}_1 & \mathbf{X}^h_{,\xi} \cdot \mathbf{t}_2 \\ \mathbf{X}^h_{,\eta} \cdot \mathbf{t}_1 & \mathbf{X}^h_{,\eta} \cdot \mathbf{t}_2 \end{bmatrix} \tag{14}$$

with

$$\begin{aligned} \mathbf{X}^h_{,\xi} &= \mathbf{G}^0_\xi + \eta\, \mathbf{G}^1 & \mathbf{G}^0_\xi &= \frac{1}{4}\sum_{I=1}^{4} \xi_I\, \mathbf{X}_I \\ \mathbf{X}^h_{,\eta} &= \mathbf{G}^0_\eta + \xi\, \mathbf{G}^1 & \mathbf{G}^0_\eta &= \frac{1}{4}\sum_{I=1}^{4} \eta_I\, \mathbf{X}_I \\ & & \mathbf{G}^1 &= \frac{1}{4}\sum_{I=1}^{4} \xi_I\, \eta_I\, \mathbf{X}_I\,. \end{aligned} \tag{15}$$

One can prove that $\mathbf{t}_3 \cdot \mathbf{G}^0_\xi = 0$ and $\mathbf{t}_3 \cdot \mathbf{G}^0_\eta = 0$ holds which shows that $\mathbf{t}_3$ is normal vector at the element center. Thus $\mathbf{t}_1$ and $\mathbf{t}_2$ span a tangent plane at the center of the element. Now we are able to express the local cartesian derivatives of the shape functions using the inverse Jacobian matrix $\mathbf{J}$. The tangent vectors $\mathbf{X}_{,\alpha}$ and the derivatives of the director vector $\mathbf{D}_{,\alpha}$ are computed considering (12) as follows

$$\mathbf{X}^h_{,\alpha} = \sum_{I=1}^{4} N_{I,\alpha}\, \mathbf{X}_I \qquad \mathbf{D}^h_{,\alpha} = \sum_{I=1}^{4} N_{I,\alpha}\, \mathbf{D}_I \qquad \begin{bmatrix} N_{I,1} \\ N_{I,2} \end{bmatrix} = \mathbf{J}^{-1} \begin{bmatrix} N_{I,\xi} \\ N_{I,\eta} \end{bmatrix}. \tag{16}$$

For arbitrary warped elements one obtains $\mathbf{X}^h_{,\alpha} = \mathbf{t}_\alpha$ at the element center, which can be shown using above orthogonality conditions. This is important in the context of the present mixed interpolation. Furthermore a local cartesian system is advantageous to verify complicated nonlinear constitutive equations. At other points of the element the vectors $\mathbf{X}^h_{,\alpha}$ are only approximately orthogonal.

The current shell middle surface is approximated in the same way

$$\begin{aligned} \mathbf{x}^h &= \sum_{I=1}^{4} N_I\, \mathbf{x}_I & \mathbf{d}^h &= \sum_{I=1}^{4} N_I\, \mathbf{d}_I \\ \mathbf{x}^h_{,\alpha} &= \sum_{I=1}^{4} N_{I,\alpha}\, \mathbf{x}_I & \mathbf{d}^h_{,\alpha} &= \sum_{I=1}^{4} N_{I,\alpha}\, \mathbf{d}_I\,, \end{aligned} \tag{17}$$

where $\mathbf{x}_I = \mathbf{X}_I + \mathbf{u}_I$ describes the current nodal position vector and $\mathbf{d}_I = \mathbf{a}_{3I}$ is obtained by an orthogonal transformation $\mathbf{a}_{kI} = \mathbf{R}_I\, \mathbf{A}_{kI}, \quad k = 1, 2, 3$. The rotation tensor $\mathbf{R}_I$ is a function of the parameters organized in the vector $\boldsymbol{\omega}_I = [\omega_{1I}, \omega_{2I}, \omega_{3I}]^T$ and is computed via Rodrigues' formula

$$\mathbf{R}_I = \mathbf{1} + \frac{\sin\omega_I}{\omega_I}\boldsymbol{\Omega}_I + \frac{1-\cos\omega_I}{\omega_I^2}\boldsymbol{\Omega}_I^2 \qquad \boldsymbol{\Omega}_I = \operatorname{skew}\boldsymbol{\omega}_I = \begin{bmatrix} 0 & -\omega_{3I} & \omega_{2I} \\ \omega_{3I} & 0 & -\omega_{1I} \\ -\omega_{2I} & \omega_{1I} & 0 \end{bmatrix} \tag{18}$$

Representation (18) is singularity free for $\omega_I = |\boldsymbol{\omega}_I| < 2\pi$ which can always be fulfilled if after a certain number of load steps a multiplicative update of the total rotation tensor is applied.

3.2 Interpolation of the Green–Lagrangean strains and associated variations

The element has to fulfil membrane and bending patch test, see e.g. [27]. As has been shown in appendix B the bending patch test – when using the present mixed interpolation for the stress resultants and shell strains – can be fulfilled with substitute shear strains defined in [23] but not with the bilinear displacement interpolation inserted in the transverse shear strains $(5)_3$. Thus the finite element interpolation of the Green–Lagrangean strains reads

$$\boldsymbol{\varepsilon}_G^h = \begin{bmatrix} \varepsilon_{11}^h \\ \varepsilon_{22}^h \\ 2\varepsilon_{12}^h \\ \kappa_{11}^h \\ \kappa_{22}^h \\ 2\kappa_{12}^h \\ \gamma_1^h \\ \gamma_2^h \end{bmatrix} = \begin{bmatrix} \frac{1}{2}\left(\mathbf{x}_{,1}^h \cdot \mathbf{x}_{,1}^h - \mathbf{X}_{,1}^h \cdot \mathbf{X}_{,1}^h\right) \\ \frac{1}{2}\left(\mathbf{x}_{,2}^h \cdot \mathbf{x}_{,2}^h - \mathbf{X}_{,2}^h \cdot \mathbf{X}_{,2}^h\right) \\ \mathbf{x}_{,1}^h \cdot \mathbf{x}_{,2}^h - \mathbf{X}_{,1}^h \cdot \mathbf{X}_{,2}^h \\ \mathbf{x}_{,1}^h \cdot \mathbf{d}_{,1}^h - \mathbf{X}_{,1}^h \cdot \mathbf{D}_{,1}^h \\ \mathbf{x}_{,2}^h \cdot \mathbf{d}_{,2}^h - \mathbf{X}_{,2}^h \cdot \mathbf{D}_{,2}^h \\ \mathbf{x}_{,1}^h \cdot \mathbf{d}_{,2}^h + \mathbf{x}_{,2}^h \cdot \mathbf{d}_{,1}^h - \mathbf{X}_{,1}^h \cdot \mathbf{D}_{,2}^h - \mathbf{X}_{,2}^h \cdot \mathbf{D}_{,1}^h \\ \mathbf{J}^{-1} \begin{Bmatrix} \frac{1}{2}[(1-\eta)\,\gamma_\xi^B + (1+\eta)\,\gamma_\xi^D \\ \frac{1}{2}[(1-\xi)\,\gamma_\eta^A + (1+\xi)\,\gamma_\eta^C] \end{Bmatrix} \end{bmatrix}. \tag{19}$$

The strains at the midside nodes A, B, C, D of the element are specified as follows

$$\begin{aligned} \gamma_\xi^M &= [\mathbf{x}_{,\xi} \cdot \mathbf{d} - \mathbf{X}_{,\xi} \cdot \mathbf{D}]^M \qquad M = B, D \\ \gamma_\eta^L &= [\mathbf{x}_{,\eta} \cdot \mathbf{d} - \mathbf{X}_{,\eta} \cdot \mathbf{D}]^L \qquad L = A, C\,, \end{aligned} \tag{20}$$

where the following quantities are given with the bilinear interpolation (12) and (17)

$$\begin{aligned} \mathbf{d}^A &= \tfrac{1}{2}(\mathbf{d}_4 + \mathbf{d}_1) & \mathbf{D}^A &= \tfrac{1}{2}(\mathbf{D}_4 + \mathbf{D}_1) \\ \mathbf{d}^B &= \tfrac{1}{2}(\mathbf{d}_1 + \mathbf{d}_2) & \mathbf{D}^B &= \tfrac{1}{2}(\mathbf{D}_1 + \mathbf{D}_2) \\ \mathbf{d}^C &= \tfrac{1}{2}(\mathbf{d}_2 + \mathbf{d}_3) & \mathbf{D}^C &= \tfrac{1}{2}(\mathbf{D}_2 + \mathbf{D}_3) \\ \mathbf{d}^D &= \tfrac{1}{2}(\mathbf{d}_3 + \mathbf{d}_4) & \mathbf{D}^D &= \tfrac{1}{2}(\mathbf{D}_3 + \mathbf{D}_4) \\ \mathbf{x}_{,\eta}^A &= \tfrac{1}{2}(\mathbf{x}_4 - \mathbf{x}_1) & \mathbf{X}_{,\eta}^A &= \tfrac{1}{2}(\mathbf{X}_4 - \mathbf{X}_1) \\ \mathbf{x}_{,\xi}^B &= \tfrac{1}{2}(\mathbf{x}_2 - \mathbf{x}_1) & \mathbf{X}_{,\xi}^B &= \tfrac{1}{2}(\mathbf{X}_2 - \mathbf{X}_1) \\ \mathbf{x}_{,\eta}^C &= \tfrac{1}{2}(\mathbf{x}_3 - \mathbf{x}_2) & \mathbf{X}_{,\eta}^C &= \tfrac{1}{2}(\mathbf{X}_3 - \mathbf{X}_2) \\ \mathbf{x}_{,\xi}^D &= \tfrac{1}{2}(\mathbf{x}_3 - \mathbf{x}_4) & \mathbf{X}_{,\xi}^D &= \tfrac{1}{2}(\mathbf{X}_3 - \mathbf{X}_4)\,. \end{aligned} \tag{21}$$

Accordingly the interpolated virtual strains read

$$\delta\boldsymbol{\varepsilon}_G^h = \begin{bmatrix} \delta\varepsilon_{11}^h \\ \delta\varepsilon_{22}^h \\ 2\delta\varepsilon_{12}^h \\ \delta\kappa_{11}^h \\ \delta\kappa_{22}^h \\ 2\delta\kappa_{12}^h \\ \delta\gamma_1^h \\ \delta\gamma_2^h \end{bmatrix} = \begin{bmatrix} \delta\mathbf{x}_{,1}^h \cdot \mathbf{x}_{,1}^h \\ \delta\mathbf{x}_{,2}^h \cdot \mathbf{x}_{,2}^h \\ \delta\mathbf{x}_{,1}^h \cdot \mathbf{x}_{,2}^h + \delta\mathbf{x}_{,2}^h \cdot \mathbf{x}_{,1}^h \\ \delta\mathbf{x}_{,1}^h \cdot \mathbf{d}_{,1}^h + \delta\mathbf{d}_{,1}^h \cdot \mathbf{x}_{,1}^h \\ \delta\mathbf{x}_{,2}^h \cdot \mathbf{d}_{,2}^h + \delta\mathbf{d}_{,2}^h \cdot \mathbf{x}_{,2}^h \\ \delta\mathbf{x}_{,1}^h \cdot \mathbf{d}_{,2}^h + \delta\mathbf{x}_{,2}^h \cdot \mathbf{d}_{,1}^h + \delta\mathbf{d}_{,1}^h \cdot \mathbf{x}_{,2}^h + \delta\mathbf{d}_{,2}^h \cdot \mathbf{x}_{,1}^h \\ \mathbf{J}^{-1} \begin{Bmatrix} \frac{1}{2}[(1-\eta)\,\delta\gamma_\xi^B + (1+\eta)\,\delta\gamma_\xi^D \\ \frac{1}{2}[(1-\xi)\,\delta\gamma_\eta^A + (1+\xi)\,\delta\gamma_\eta^C] \end{Bmatrix} \end{bmatrix} \tag{22}$$

with

$$\begin{aligned} \delta\gamma_\xi^M &= [\delta\mathbf{x}_{,\xi}\cdot\mathbf{d}+\mathbf{x}_{,\xi}\cdot\delta\mathbf{d}]^M & M &= B, D \\ \delta\gamma_\eta^L &= [\delta\mathbf{x}_{,\eta}\cdot\mathbf{d}+\mathbf{x}_{,\eta}\cdot\delta\mathbf{d}]^L & L &= A, C\,, \end{aligned} \tag{23}$$

where $\delta\mathbf{x}_{,\xi}\,, \delta\mathbf{x}_{,\eta}\,, \delta\mathbf{d}$ are evaluated at the midside nodes considering (21).
The virtual vectors $\delta\mathbf{x}^h_{,\alpha}$ and $\delta\mathbf{d}^h_{,\alpha}$ using (17) are determined

$$\delta\mathbf{x}^h_{,\alpha} = \sum_{I=1}^{4} N_{I,\alpha}\,\delta\mathbf{u}_I \qquad \delta\mathbf{d}^h_{,\alpha} = \sum_{I=1}^{4} N_{I,\alpha}\,\delta\mathbf{d}_I\,, \tag{24}$$

with the virtual nodal displacements $\delta\mathbf{u}_I$ and

$$\delta\mathbf{d}_I = \delta\mathbf{w}_I\times\mathbf{d}_I = \mathbf{W}_I^T\,\delta\mathbf{w}_I \qquad \mathbf{W}_I = \operatorname{skew}\mathbf{d}_I \tag{25}$$

where according to [30]

$$\delta\mathbf{w}_I = \mathbf{H}_I\,\delta\boldsymbol{\omega}_I\,, \qquad \mathbf{H}_I = \mathbf{1} + \frac{1-\cos\omega_I}{\omega_I^2}\,\boldsymbol{\Omega}_I + \frac{\omega_I-\sin\omega_I}{\omega_I^3}\,\boldsymbol{\Omega}_I^2\,. \tag{26}$$

The coefficients of $\boldsymbol{\Omega}_I$ and $\boldsymbol{\Omega}_I^2$ possess the limit values $1/2$ and $1/6$ for $\omega_I \to 0$.
At nodes which are not positioned on intersections a drilling stiffness is not available and a transformation of the virtual rotation vector to the local coordinate system is necessary:

$$\delta\boldsymbol{\omega}_I = \mathbf{T}_{3I}\,\delta\boldsymbol{\beta}_I \qquad \begin{aligned} \mathbf{T}_{3I} &= \begin{cases} \mathbf{1}_3 & \text{for nodes on shell intersections} \\ [\mathbf{a}_{1I}, \mathbf{a}_{2I}]_{(3\times2)} & \text{for all other nodes} \end{cases} \\ \delta\boldsymbol{\beta}_I &= \begin{cases} [\delta\beta_{xI}, \delta\beta_{yI}, \delta\beta_{zI}]^T & \text{for nodes on shell intersections} \\ [\delta\beta_{1I}, \delta\beta_{2I}]^T & \text{for all other nodes} \end{cases} \end{aligned} \tag{27}$$

where $\delta\beta_{\alpha I}$ denote local rotations. Furthermore the drilling degree of freedom is fixed, thus $\delta\beta_{3I} = 0$. The element possesses six degrees of freedom at all nodes on intersections and five at all other nodes. In this context we also refer to [28, 29].
Next combining (25) – (27) we obtain

$$\delta\mathbf{d}_I = \mathbf{T}_I\,\delta\boldsymbol{\beta}_I \qquad \mathbf{T}_I = \mathbf{W}_I^T\mathbf{H}_I\mathbf{T}_{3I} \tag{28}$$

Thus we are able to summarize the finite element approximation of the virtual shell strains (22) considering (23) - (28)

$$\begin{bmatrix} \delta\varepsilon_{11}^h \\ \delta\varepsilon_{22}^h \\ 2\delta\varepsilon_{12}^h \\ \delta\kappa_{11}^h \\ \delta\kappa_{22}^h \\ 2\delta\kappa_{12}^h \\ \delta\gamma_1^h \\ \delta\gamma_2^h \end{bmatrix} = \sum_{I=1}^{4} \begin{bmatrix} N_{I,1}\,\mathbf{x}_{,1}^T & \mathbf{0} \\ N_{I,2}\,\mathbf{x}_{,2}^T & \mathbf{0} \\ N_{I,1}\,\mathbf{x}_{,2}^T + N_{I,2}\,\mathbf{x}_{,1}^T & \mathbf{0} \\ N_{I,1}\,\mathbf{d}_{,1}^T & N_{I,1}\,\mathbf{b}_{I1}^T \\ N_{I,2}\,\mathbf{d}_{,2}^T & N_{I,2}\,\mathbf{b}_{I2}^T \\ N_{I,1}\,\mathbf{d}_{,2}^T + N_{I,2}\,\mathbf{d}_{,1}^T & N_{I,1}\,\mathbf{b}_{I2}^T + N_{I,2}\,\mathbf{b}_{I1}^T \\ \mathbf{J}^{-1}\begin{Bmatrix} N_{I,\xi}\,\mathbf{d}_M^T \\ N_{I,\eta}\,\mathbf{d}_L^T \end{Bmatrix} & \mathbf{J}^{-1}\begin{Bmatrix} N_{I,\xi}\,\xi_I\,\mathbf{b}_M^T \\ N_{I,\eta}\,\eta_I\,\mathbf{b}_L^T \end{Bmatrix} \end{bmatrix} \begin{bmatrix} \delta\mathbf{u}_I \\ \delta\boldsymbol{\beta}_I \end{bmatrix} \tag{29}$$

$$\delta\boldsymbol{\varepsilon}_G^h = \sum_{I=1}^{4} \mathbf{B}_I\,\delta\mathbf{v}_I$$

with $\mathbf{b}_{I\alpha} = \mathbf{T}_I^T\,\mathbf{x}_{,\alpha}$, $\mathbf{b}_M = \mathbf{T}_I^T\,\mathbf{x}^M_{,\xi}$ and $\mathbf{b}_L = \mathbf{T}_I^T\,\mathbf{x}^L_{,\eta}$. The allocation of the midside nodes to the corner nodes is given by

$$(I, M, L) \in \{(1, B, A); (2, B, C); (3, D, C); (4, D, A)\}\,. \tag{30}$$

To alleviate the notation the subscript h is omitted in the matrix.

3.3 Second variation of the functional

Assuming conservative external loads $\bar{\mathbf{p}}$ and $\bar{\mathbf{t}}$ the second variation of the functional yields

$$Dg \cdot \Delta\boldsymbol{\theta}^h = \int_{(\Omega)} [\delta\boldsymbol{\varepsilon}^{hT}(\mathbf{C}\,\Delta\boldsymbol{\varepsilon}^h - \Delta\boldsymbol{\sigma}^h) + \delta\boldsymbol{\sigma}^{hT}(\Delta\boldsymbol{\varepsilon}^h_G - \Delta\boldsymbol{\varepsilon}^h) + \delta\boldsymbol{\varepsilon}^{hT}_G\Delta\boldsymbol{\sigma}^h + \Delta\delta\boldsymbol{\varepsilon}^{hT}_G\boldsymbol{\sigma}^h]\,dA \tag{31}$$

with $\mathbf{C} := \partial^2_{\boldsymbol{\varepsilon}} W$. The linearized strains $\Delta\boldsymbol{\varepsilon}^h_G$ are defined with (22) replacing the operator δ by Δ whereas the linearized virtual shell strains are given with

$$\Delta\delta\boldsymbol{\varepsilon}^h_G = \begin{bmatrix} \Delta\delta\varepsilon^h_{11} \\ \Delta\delta\varepsilon^h_{22} \\ 2\Delta\delta\varepsilon^h_{12} \\ \Delta\delta\kappa^h_{11} \\ \Delta\delta\kappa^h_{22} \\ 2\Delta\delta\kappa^h_{12} \\ \\ \Delta\delta\gamma^h_1 \\ \Delta\delta\gamma^h_2 \end{bmatrix} = \begin{bmatrix} \delta\mathbf{x}^h_{,1}\cdot\Delta\mathbf{x}^h_{,1} \\ \delta\mathbf{x}^h_{,2}\cdot\Delta\mathbf{x}^h_{,2} \\ \delta\mathbf{x}^h_{,1}\cdot\Delta\mathbf{x}^h_{,2} + \delta\mathbf{x}^h_{,2}\cdot\Delta\mathbf{x}^h_{,1} \\ \delta\mathbf{x}^h_{,1}\cdot\Delta\mathbf{d}^h_{,1} + \delta\mathbf{d}^h_{,1}\cdot\Delta\mathbf{x}^h_{,1} + \mathbf{x}^h_{,1}\cdot\Delta\delta\mathbf{d}^h_{,1} \\ \delta\mathbf{x}^h_{,2}\cdot\Delta\mathbf{d}^h_{,2} + \delta\mathbf{d}^h_{,2}\cdot\Delta\mathbf{x}^h_{,2} + \mathbf{x}^h_{,2}\cdot\Delta\delta\mathbf{d}^h_{,2} \\ \delta\mathbf{x}^h_{,1}\cdot\Delta\mathbf{d}^h_{,2} + \delta\mathbf{x}^h_{,2}\cdot\Delta\mathbf{d}^h_{,1} + \delta\mathbf{d}^h_{,1}\cdot\Delta\mathbf{x}^h_{,2} + \delta\mathbf{d}^h_{,2}\cdot\Delta\mathbf{x}^h_{,1} \\ \quad + \mathbf{x}^h_{,1}\cdot\Delta\delta\mathbf{d}^h_{,2} + \mathbf{x}^h_{,2}\cdot\Delta\delta\mathbf{d}^h_{,1} \\ \mathbf{J}^{-1}\left\{ \begin{array}{c} \frac{1}{2}[(1-\eta)\,\Delta\delta\gamma^B_\xi + (1+\eta)\,\Delta\delta\gamma^D_\xi \\ \frac{1}{2}[(1-\xi)\,\Delta\delta\gamma^A_\eta + (1+\xi)\,\Delta\delta\gamma^C_\eta] \end{array} \right\} \end{bmatrix} \tag{32}$$

with

$$\begin{aligned} \Delta\delta\gamma^M_\xi &= [\delta\mathbf{x}_{,\xi}\cdot\Delta\mathbf{d} + \Delta\mathbf{x}_{,\xi}\cdot\delta\mathbf{d} + \mathbf{x}_{,\xi}\cdot\Delta\delta\mathbf{d}]^M \qquad M = B, D \\ \Delta\delta\gamma^L_\eta &= [\delta\mathbf{x}_{,\eta}\cdot\Delta\mathbf{d} + \Delta\mathbf{x}_{,\eta}\cdot\delta\mathbf{d} + \mathbf{x}_{,\eta}\cdot\Delta\delta\mathbf{d}]^L \qquad L = A, C \end{aligned} \tag{33}$$

The second variation of the current orthogonal base system has been derived in [30], see appendix A. In the following representation the constants c_i introduced in [30] are simplified and the Taylor series expansion is given. With an arbitrary vector $\mathbf{h}_I \in \boldsymbol{R}^3$ and $\mathbf{b}_I = \mathbf{d}_I \times \mathbf{h}_I$ we obtain

$$\begin{aligned} \mathbf{h}_I \cdot \Delta\delta\mathbf{d}_I &= \delta\mathbf{w}_I \cdot \mathbf{M}_I\,\Delta\mathbf{w}_I \\ \mathbf{M}_I(\mathbf{h}_I) &= \frac{1}{2}(\mathbf{d}_I \otimes \mathbf{h}_I + \mathbf{h}_I \otimes \mathbf{d}_I) + \frac{1}{2}(\mathbf{t}_I \otimes \boldsymbol{\omega}_I + \boldsymbol{\omega}_I \otimes \mathbf{t}_I) + c_{10}\mathbf{1} \\ \mathbf{t}_I &= -c_3\,\mathbf{b}_I + c_{11}\,(\mathbf{b}_I \cdot \boldsymbol{\omega}_I)\,\boldsymbol{\omega}_I \qquad c_{10} = \bar{c}_{10}\,(\mathbf{b}_I \cdot \boldsymbol{\omega}_I) - (\mathbf{d}_I \cdot \mathbf{h}_I) \\ c_3 &= \frac{\omega_I\,\sin\omega_I + 2\,(\cos\omega_I - 1)}{\omega_I^2\,(\cos\omega_I - 1)} = \frac{1}{6}\,(1 + \frac{1}{60}\,\omega_I^2) + O(\omega_I^4) \\ \bar{c}_{10} &= \frac{\sin\omega_I - \omega_I}{2\omega_I\,(\cos\omega_I - 1)} = \frac{1}{6}\,(1 + \frac{1}{30}\,\omega_I^2) + O(\omega_I^4) \\ c_{11} &= \frac{4\,(\cos\omega_I - 1) + \omega_I^2 + \omega_I\sin\omega_I}{2\,\omega_I^4\,(\cos\omega_I - 1)} = -\frac{1}{360}\,(1 + \frac{1}{21}\,\omega_I^2) + O(\omega_I^4) \end{aligned} \tag{34}$$

To avoid numerical difficulties the series expansion of the coefficients should be used if ω_I approaches zero. Hence the finite element formulation of the linearized virtual membrane strains and curvatures considering (34) reads

$$\begin{aligned}
\Delta\delta\varepsilon_{\alpha\beta} &= \sum_{I=1}^{4}\sum_{K=1}^{4} \frac{1}{2}(N_{I,\alpha}\, N_{K,\beta} + N_{I,\beta}\, N_{K,\alpha})\, \delta\mathbf{u}_I \cdot \Delta\mathbf{u}_K \\
\Delta\delta\kappa_{\alpha\beta} &= \sum_{I=1}^{4}\sum_{K=1}^{4} \{\frac{1}{2}(N_{I,\alpha}\, N_{K,\beta} + N_{I,\beta}\, N_{K,\alpha})\, \delta\mathbf{u}_I \cdot \Delta\mathbf{d}_K \\
&\qquad + \frac{1}{2}(N_{I,\alpha}\, N_{K,\beta} + N_{I,\beta}\, N_{K,\alpha})\, \delta\mathbf{d}_I \cdot \Delta\mathbf{u}_K \\
&\qquad + \delta_{IK}\frac{1}{2}\left[\delta\mathbf{w}_I \cdot (N_{I,\alpha}\, \mathbf{M}_I(\mathbf{x}_{,\beta}) + N_{I,\beta}\, \mathbf{M}_I(\mathbf{x}_{,\alpha}))\, \Delta\mathbf{w}_K\right]\}
\end{aligned} \tag{35}$$

where δ_{IK} denotes the Kronecker delta.
Finally, we specify the product $\Delta\delta\boldsymbol{\varepsilon}_G^{hT}\boldsymbol{\sigma}^h$ with the independent stress resultants $\boldsymbol{\sigma}^h = [n^{11}, n^{22}, n^{12}, m^{11}, m^{22}, m^{12}, q^1, q^2]^T$ using (32) - (35)

$$\begin{aligned}
\Delta\delta\boldsymbol{\varepsilon}_G^{hT}\boldsymbol{\sigma}^h &= \sum_{I}^{4}\sum_{K}^{4} \delta\mathbf{v}_I^T\, \mathbf{k}_{\sigma IK}\, \Delta\mathbf{v}_K \\
&= \sum_{I}^{4}\sum_{K}^{4} \begin{bmatrix} \delta\mathbf{u}_I \\ \delta\boldsymbol{\beta}_I \end{bmatrix}^T \begin{bmatrix} \hat{n}_{IK}\mathbf{1} & (\hat{m}_{IK} + \hat{q}_{IK}^{uw})\mathbf{T}_K \\ (\hat{m}_{IK} + \hat{q}_{IK}^{wu})\mathbf{T}_I^T & \delta_{IK}\,\hat{\mathbf{M}}_I(\mathbf{h}_I) \end{bmatrix} \begin{bmatrix} \Delta\mathbf{u}_K \\ \Delta\boldsymbol{\beta}_K \end{bmatrix}
\end{aligned} \tag{36}$$

The matrix $\mathbf{k}_{\sigma IK}$ is determined with

$$\begin{aligned}
\hat{n}_{IK} &= n^{11}\, N_{I,1}\, N_{K,1} + n^{22}\, N_{I,2}\, N_{K,2} + n^{12}\, (N_{I,1}\, N_{K,2} + N_{I,2}\, N_{K,1}) \\
\hat{m}_{IK} &= m^{11}\, N_{I,1}\, N_{K,1} + m^{22}\, N_{I,2}\, N_{K,2} + m^{12}\, (N_{I,1}\, N_{K,2} + N_{I,2}\, N_{K,1}) \\
\hat{q}_{IK}^{uw} &= \tfrac{1}{2}(q^\xi\, N_{I,\xi}\, f_{IK}^1 + q^\eta\, N_{I,\eta}\, f_{IK}^2) \\
\hat{q}_{IK}^{wu} &= \tfrac{1}{2}(q^\xi\, N_{K,\xi}\, f_{IK}^1 + q^\eta\, N_{K,\eta}\, f_{IK}^2) \\
\hat{\mathbf{M}}_I &= \mathbf{T}_{3I}^T\, \mathbf{H}_I^T\, \mathbf{M}_I(\mathbf{h}_I)\, \mathbf{H}_I\, \mathbf{T}_{3I} \\
\mathbf{h}_I &= m^{11}\, N_{I,1}\, \mathbf{x}_{,1}^h + m^{22}\, N_{I,2}\, \mathbf{x}_{,2}^h + m^{12}\, (N_{I,2}\, \mathbf{x}_{,1}^h + N_{I,1}\, \mathbf{x}_{,2}^h) \\
&\quad + q^\xi\, N_{I,\xi}\, \xi_I \mathbf{x}_{,\xi}^M + q^\eta\, N_{I,\eta}\, \eta_I \mathbf{x}_{,\eta}^L
\end{aligned} \tag{37}$$

$$[f_{IK}^1] = \begin{bmatrix} 1 & 1 & 0 & 0 \\ 1 & 1 & 0 & 0 \\ 0 & 0 & 1 & 1 \\ 0 & 0 & 1 & 1 \end{bmatrix} \qquad [f_{IK}^2] = \begin{bmatrix} 1 & 0 & 0 & 1 \\ 0 & 1 & 1 & 0 \\ 0 & 1 & 1 & 0 \\ 1 & 0 & 0 & 1 \end{bmatrix} \qquad \begin{bmatrix} q^\xi \\ q^\eta \end{bmatrix} = \mathbf{J}^{-T} \begin{bmatrix} q^1 \\ q^2 \end{bmatrix}.$$

where $\mathbf{M}_I(\mathbf{h}_I)$ is defined in (34) and the allocation of the midside nodes M, L to the corner nodes in (30).

3.4 Interpolation of the stress resultants and shell strains

Regarding the requirements on the interpolation functions to fulfil patch test and to ensure stability of the discrete equations according to appendix B the independent field of stress

resultants $\boldsymbol{\sigma}$ is approximated as follows

$$\begin{aligned}
\boldsymbol{\sigma}^h &= \mathbf{N}_\sigma\,\hat{\boldsymbol{\sigma}} & \mathbf{N}_\sigma &= [\mathbf{1}_8, \tilde{\mathbf{N}}_\sigma] \\
\tilde{\mathbf{N}}_\sigma &= \begin{bmatrix} \mathbf{N}_\sigma^m & \mathbf{0} & \mathbf{0} \\ \mathbf{0} & \mathbf{N}_\sigma^b & \mathbf{0} \\ \mathbf{0} & \mathbf{0} & \mathbf{N}_\sigma^s \end{bmatrix} & \mathbf{N}_\sigma^m &= \mathbf{N}_\sigma^b \\
\mathbf{N}_\sigma^m &= \begin{bmatrix} J_{11}^0 J_{11}^0(\eta-\bar\eta) & J_{21}^0 J_{21}^0(\xi-\bar\xi) \\ J_{12}^0 J_{12}^0(\eta-\bar\eta) & J_{22}^0 J_{22}^0(\xi-\bar\xi) \\ J_{11}^0 J_{12}^0(\eta-\bar\eta) & J_{21}^0 J_{22}^0(\xi-\bar\xi) \end{bmatrix} & \mathbf{N}_\sigma^s &= \begin{bmatrix} J_{11}^0(\eta-\bar\eta) & J_{21}^0(\xi-\bar\xi) \\ J_{12}^0(\eta-\bar\eta) & J_{22}^0(\xi-\bar\xi) \end{bmatrix}
\end{aligned} \tag{38}$$

Here, we denote by $\mathbf{1}_8$ an eight order unit matrix. The vector $\hat{\boldsymbol{\sigma}}$ contains 8 parameters for the constant part and 6 parameters for the varying part of the stress field, respectively. The interpolation of the membrane forces and bending moments corresponds to the procedure in [31], see also the original approach for plane stress problems with $\bar\xi = \bar\eta = 0$ in [32]. The transformation coefficients $J_{\alpha\beta}^0 = J_{\alpha\beta}(\xi = 0, \eta = 0)$ are the components of the Jacobian matrix $\mathbf{J}$ (14) evaluated at the element center. Due to the constants

$$\bar\xi = \frac{1}{A_e}\int\limits_{(\Omega_e)} \xi\, dA \qquad \bar\eta = \frac{1}{A_e}\int\limits_{(\Omega_e)} \eta\, dA \qquad A_e = \int\limits_{(\Omega_e)} dA \tag{39}$$

the linear functions are orthogonal to the constant function which yields partly decoupled matrices. In this context we refer also to [33] in the case of a plate formulation.
The independent shell strains are approximated with 14 parameters in $\hat{\boldsymbol{\varepsilon}}$

$$\begin{aligned}
\boldsymbol{\varepsilon}^h &= \mathbf{N}_\varepsilon\,\hat{\boldsymbol{\varepsilon}} & \mathbf{N}_\varepsilon &= [\mathbf{1}_8, \tilde{\mathbf{N}}_\varepsilon] \\
\tilde{\mathbf{N}}_\varepsilon &= \begin{bmatrix} \mathbf{N}_\varepsilon^m & \mathbf{0} & \mathbf{0} \\ \mathbf{0} & \mathbf{N}_\varepsilon^b & \mathbf{0} \\ \mathbf{0} & \mathbf{0} & \mathbf{N}_\varepsilon^s \end{bmatrix} & \mathbf{N}_\varepsilon^m &= \mathbf{N}_\varepsilon^b \\
\mathbf{N}_\varepsilon^m &= \begin{bmatrix} J_{11}^0 J_{11}^0(\eta-\bar\eta) & J_{21}^0 J_{21}^0(\xi-\bar\xi) \\ J_{12}^0 J_{12}^0(\eta-\bar\eta) & J_{22}^0 J_{22}^0(\xi-\bar\xi) \\ 2J_{11}^0 J_{12}^0(\eta-\bar\eta) & 2J_{21}^0 J_{22}^0(\xi-\bar\xi) \end{bmatrix} & \mathbf{N}_\varepsilon^s &= \mathbf{N}_\sigma^s\,.
\end{aligned} \tag{40}$$

Thus, the independent stresses and strains are interpolated with the same shape functions. We remark that (38) and (40) contain a transformation of the contravariant tensor components to the local cartesian coordinate system at the element center.

3.5 Linearized variational formulation

Inserting above interpolations for the displacements, stresses and strains into the linearized stationary condition yields

$$\begin{aligned}
L\left[g(\boldsymbol{\theta}^h, \delta\boldsymbol{\theta}^h), \Delta\boldsymbol{\theta}^h\right] &:= g(\boldsymbol{\theta}^h, \delta\boldsymbol{\theta}^h) + Dg\cdot\Delta\boldsymbol{\theta}^h \\
&= \sum_{e=1}^{numel} \begin{bmatrix} \delta\mathbf{v} \\ \delta\hat{\boldsymbol{\varepsilon}} \\ \delta\hat{\boldsymbol{\sigma}} \end{bmatrix}_e^T \left\{ \begin{bmatrix} \mathbf{k}_g & \mathbf{0} & \mathbf{G}^T \\ \mathbf{0} & \mathbf{H} & -\mathbf{F} \\ \mathbf{G} & -\mathbf{F}^T & \mathbf{0} \end{bmatrix} \begin{bmatrix} \Delta\mathbf{v} \\ \Delta\hat{\boldsymbol{\varepsilon}} \\ \Delta\hat{\boldsymbol{\sigma}} \end{bmatrix} + \begin{bmatrix} \mathbf{f}^i - \mathbf{f}^a \\ \mathbf{f}^e \\ \mathbf{f}^s \end{bmatrix} \right\}_e
\end{aligned} \tag{41}$$

where *numel* denotes the total number of finite shell elements to discretize the problem. The following element matrices are defined with $\mathbf{B} = [\mathbf{B}_1, \mathbf{B}_2, \mathbf{B}_3, \mathbf{B}_4]$ from(29) and $\mathbf{k}_\sigma$ introduced in (36)

$$\begin{aligned} \mathbf{k}_g &= \int_{\Omega_e} \mathbf{k}_\sigma \, dA & \mathbf{f}^i &= \int_{\Omega_e} \mathbf{B}^T \boldsymbol{\sigma}^h \, dA = \mathbf{G}^T \hat{\boldsymbol{\sigma}} \\ \mathbf{H} &= \int_{\Omega_e} \mathbf{N}_\varepsilon^T \, \mathbf{C} \, \mathbf{N}_\varepsilon \, dA & \mathbf{f}^e &= \int_{\Omega_e} \mathbf{N}_\varepsilon^T \, \partial_{\boldsymbol{\varepsilon}} W \, dA - \mathbf{F} \, \hat{\boldsymbol{\sigma}} \\ \mathbf{F} &= \int_{\Omega_e} \mathbf{N}_\varepsilon^T \, \mathbf{N}_\sigma \, dA & \mathbf{f}^s &= \int_{\Omega_e} \mathbf{N}_\sigma^T \, \boldsymbol{\varepsilon}_G^h \, dA - \mathbf{F}^T \, \hat{\boldsymbol{\varepsilon}} \\ \mathbf{G} &= \int_{\Omega_e} \mathbf{N}_\sigma^T \, \mathbf{B} \, dA \,. \end{aligned} \tag{42}$$

The vector of the external loads $\mathbf{f}^a$ corresponds to the standard displacement formulation. The computation of the stress resultants $\partial_{\boldsymbol{\varepsilon}} W$ and linearized stress resultants $\mathbf{C}$ is explicitly described in appendix C. This requires the fulfillment of the plane stress condition at each integration point. The integrals in (39) and (42) are computed numerically using a 2×2 Gauss integration scheme considering $dA = |\mathbf{X}^h_{,\xi} \times \mathbf{X}^h_{,\eta}| \, d\xi d\eta$. Due to the introduced constants $\bar{\xi}$ and $\bar{\eta}$ the matrix $\mathbf{F}$ possesses a diagonal structure, see appendix D. In case of linear elasticity one can show, that $\mathbf{f}^e \equiv \mathbf{0}$ holds. For the geometrical and physical linear case an analytical integration of all matrices is possible along with a flat projection, see [34] on basis of a Hellinger–Reissner functional.

We continue with $L[g(\boldsymbol{\theta}^h, \delta\boldsymbol{\theta}^h), \Delta\boldsymbol{\theta}^h] = 0$ where $\delta\boldsymbol{\theta}^h \neq \mathbf{0}$ and obtain

$$\begin{bmatrix} \mathbf{k}_g & \mathbf{0} & \mathbf{G}^T \\ \mathbf{0} & \mathbf{H} & -\mathbf{F} \\ \mathbf{G} & -\mathbf{F}^T & \mathbf{0} \end{bmatrix} \begin{bmatrix} \Delta\mathbf{v} \\ \Delta\hat{\boldsymbol{\varepsilon}} \\ \Delta\hat{\boldsymbol{\sigma}} \end{bmatrix} = - \begin{bmatrix} \mathbf{f}^i - \mathbf{f}^a \\ \mathbf{f}^e \\ \mathbf{f}^s \end{bmatrix} \tag{43}$$

Since the stresses and strains are interpolated discontinuously across the element boundaries the parameters $\Delta\hat{\boldsymbol{\varepsilon}}$ and $\Delta\hat{\boldsymbol{\sigma}}$ can be eliminated on the element level

$$\begin{aligned} \Delta\hat{\boldsymbol{\varepsilon}} &= \mathbf{F}^{T-1} \, (\mathbf{G} \, \Delta\mathbf{v} + \mathbf{f}^s) \\ \Delta\hat{\boldsymbol{\sigma}} &= \mathbf{F}^{-1} \, (\mathbf{H} \, \Delta\hat{\boldsymbol{\varepsilon}} + \mathbf{f}^e) \,. \end{aligned} \tag{44}$$

Due to the special structure of $\mathbf{F}$ the inverse matrix can easily be computed. Only submatrices of order two have to be inverted. Inserting (44) in $(43)_1$ yields the tangential element stiffness matrix $\mathbf{k}_T^e$ and the element residual vector $\hat{\mathbf{f}}$

$$\begin{aligned} L\,[g(\boldsymbol{\theta}^h, \delta\boldsymbol{\theta}^h), \Delta\boldsymbol{\theta}^h] &= \sum_{e=1}^{numel} \delta\mathbf{v}^T (\mathbf{k}_T^e \, \Delta\mathbf{v} + \hat{\mathbf{f}}) = 0 \\ \mathbf{k}_T^e &= \mathbf{G}^T \, \hat{\mathbf{H}} \, \mathbf{G} + \mathbf{k}_g \qquad\qquad \hat{\mathbf{H}} = \mathbf{F}^{-1} \, \mathbf{H} \, \mathbf{F}^{T-1} \\ \hat{\mathbf{f}} &= \mathbf{G}^T \, (\hat{\boldsymbol{\sigma}} + \hat{\mathbf{H}} \, \mathbf{f}^s + \mathbf{F}^{-1} \, \mathbf{f}^e) - \mathbf{f}^a \end{aligned} \tag{45}$$

With the condensed element matrices the global matrices are obtained

$$\mathbf{K}_T = \mathop{\mathbf{A}}_{e=1}^{numel} \mathbf{k}_T^e \qquad\qquad \hat{\mathbf{F}} = \mathop{\mathbf{A}}_{e=1}^{numel} \hat{\mathbf{f}} \,. \tag{46}$$

where $\mathbf{A}$ denotes the standard assembly operator. The solution of the global system of equations yields the increment of the global displacement vector $\Delta\mathbf{V} = -\mathbf{K}_T^{-1}\,\hat{\mathbf{F}}$ and thus the increments $\Delta\mathbf{u}_K$ and $\Delta\boldsymbol{\beta}_K$ at each node. Here, one has to consider transformation (27)

$$\Delta\boldsymbol{\omega}_K = \mathbf{T}_{3K}\,\Delta\boldsymbol{\beta}_K \qquad \mathbf{T}_{3K} \;=\; \begin{cases} \mathbf{1}_3 & \text{for nodes on shell intersections} \\ [\mathbf{a}_{1K}, \mathbf{a}_{2K}]_{(3\times 2)} & \text{for all other nodes} \end{cases} \tag{47}$$

The update of the nodal displacements is performed in a standard way on the system level,

$$\begin{aligned} \mathbf{u}_K &\Longleftarrow \mathbf{u}_K + \Delta\mathbf{u}_K \\ \boldsymbol{\omega}_K &\Longleftarrow \boldsymbol{\omega}_K + \Delta\boldsymbol{\omega}_K \end{aligned} \qquad \hat{\boldsymbol{\sigma}} \Longleftarrow \hat{\boldsymbol{\sigma}} + \Delta\hat{\boldsymbol{\sigma}} \qquad\qquad \hat{\boldsymbol{\varepsilon}} \Longleftarrow \hat{\boldsymbol{\varepsilon}} + \Delta\hat{\boldsymbol{\varepsilon}}\,, \tag{48}$$

whereas the stress and strain parameters are updated on the element level using (44). For this purpose the matrices which are necessary for the update have to be stored for each element.

4 Examples

The derived element formulation has been implemented in an extended version of the general purpose finite element program FEAP, see Zienkiewicz and Taylor [35].

4.1 Membrane and bending patch test

As a first example we investigate the element behaviour within a constant membrane and bending patch test as depicted in Fig. 2, see also [36]. A rectangular plate of length a and width b is supported at three corners. We consider in–plane loading and bending loading denoted by load case 1 and 2, respectively. Both, membrane and bending patch test are fulfilled by the present element with constant normal forces $n_x = 1, n_y = n_{xy} = 0$ (load case 1) and constant bending moments $m_x = m_y = m_{xy} = 1$ (load case 2). In the case of solid shell elements we refer to [19].

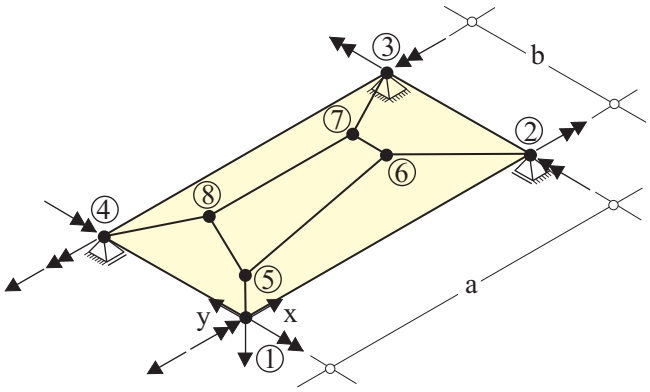

Load case	1	2		
Node	F_x	F_z	$\bar{m}_x$	$\bar{m}_y$
1	-20	-2	20	-10
2	0	0	20	10
3	0	0	-20	10
4	-20	0	-20	-10

$$
\begin{aligned}
a &= 40 \\
b &= 20 \\
h &= 0.1 \\
E &= 10^6 \\
\nu &= 0.3
\end{aligned}
$$

Figure 2: Rectangular plate, patch of 5 elements

4.2 Linear test problem: Twisted beam

The clamped beam twisted 90° subjected to two different concentrated loads at the tip was originally introduced by MacNeal and Harder [36]. A more demanding thin shell version was proposed by Jetteur [37] and is investigated in this paper.
The linear elastic example is chosen to test the assess of warping on the performance of shell elements. Two load cases are discussed. Load case 1 is a unit shear load in width direction whereas load case 2 is a unit shear load in thickness direction, see Fig. 3. All computed and reported tip displacements in load direction are normalized with respect to our converged solutions 1.387 (load case 1) and 0.3429 (load case 2), see also [38], and are presented in Tabs. 1 and 2. The linear version [34] based on a Hellinger–Reissner functional with flat projection and warping transformation exhibits a slightly oscillating convergence behaviour where this is not the case for the present element. The displacements u_z and u_y are plotted for the respective load case on the deformed configurations in Fig. 4.

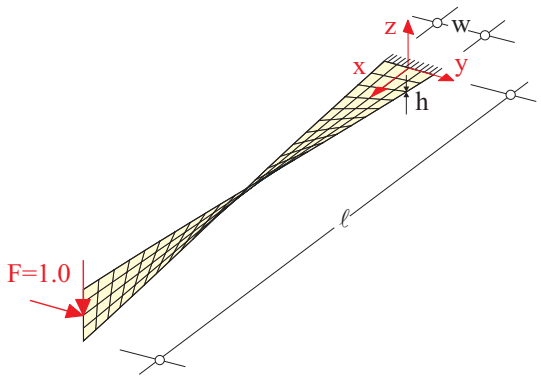

$$
\begin{aligned}
l &= 12 \\
w &= 1.1 \\
h &= 0.05 \\
E &= 29 \cdot 10^6 \\
\nu &= 0.22 \\
F &= 1.0
\end{aligned}
$$

Figure 3: Twisted beam: geometrical and material data

Table 1: Load case 1 normalized displacement u_z for different elements

Mesh	El.	Simo [31]	Taylor [38]	Sauer [17]	Gruttmann/ Wagner [34]	Present
1*6	6	99.4	100.1	99.5	102.0	99.6
2*12	24	100.0	100.2	99.7	100.6	99.7
4*24	96	100.1	100.1	99.9	99.3	99.9
8*48	384	100.2	100.0	100.0	100.0	100.0

Table 2: Load case 2 normalized displacement u_y for different elements

Mesh	El.	Simo [31]	Taylor [38]	Sauer [17]	Gruttmann/ Wagner [34]	Present
1*6	6	95.1	102.1	94.0	104.4	94.0
2*12	24	98.7	101.1	98.5	100.5	98.5
4*24	96	99.8	100.2	99.6	99.4	99.6
8*48	384	100.1	100.0	99.9	100.0	100.0

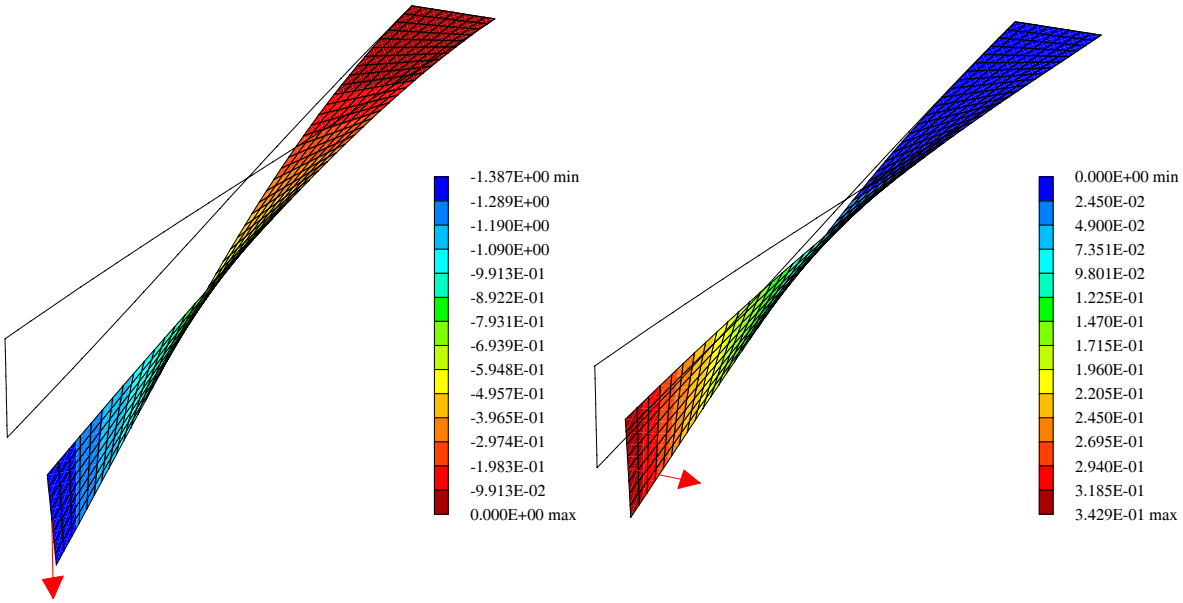

Figure 4: Deformed configurations for load case 1 and 2 and with displacements u_z and u_y

4.3 Hemispherical shell with a 18° hole

The hemispherical shell with a 18° hole under opposite loads is a standard example in linear and nonlinear shell analysis. A quarter of the shell is modelled with 16×16 elements using symmetry conditions, see Fig. 5. The material properties are $E = 6.825 \cdot 10^7$ and $\nu = 0.3$, the radius is $R = 10$ and the thickness is $h = 0.04$. The complete load deflection curve for a 16×16 mesh is presented in Fig. 6. Results for the present element – which are nearly identical with the EAS–shell [17] – show a very good agreement with those reported in [9]. Starting with $F = 0$ a maximum load step of 40 is possible with the EAS–shell [17]. For this load step the norm of the residual vector within the equilibrium iteration is given in Fig. 6 and again shows the superior behaviour of the new element. It is important to note that the relative large number of 19 iterations occurs for a finite rotation element along with large rigid body motions and is not a consequence of the enhanced strain formulation. Moreover, using the present element, the total load of $F = 100$ can be applied in a single load step with 17 iterations.

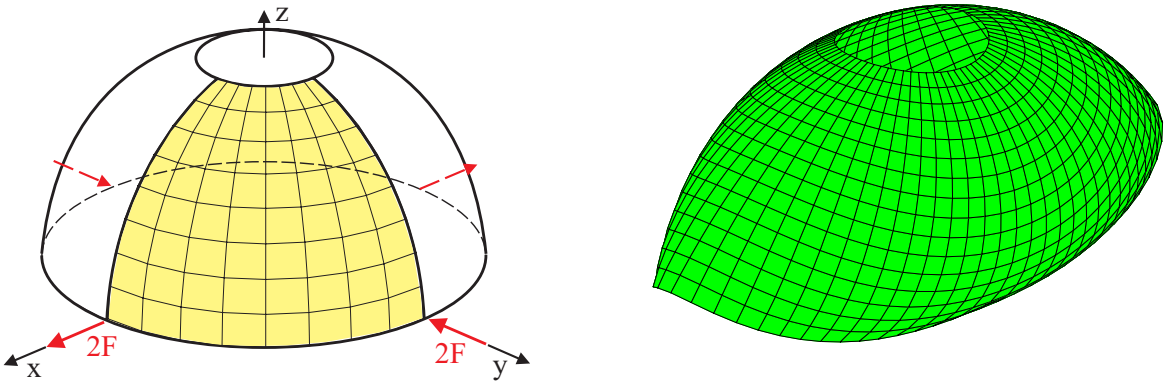

Figure 5: Hemispherical shell and deformed mesh for F=100

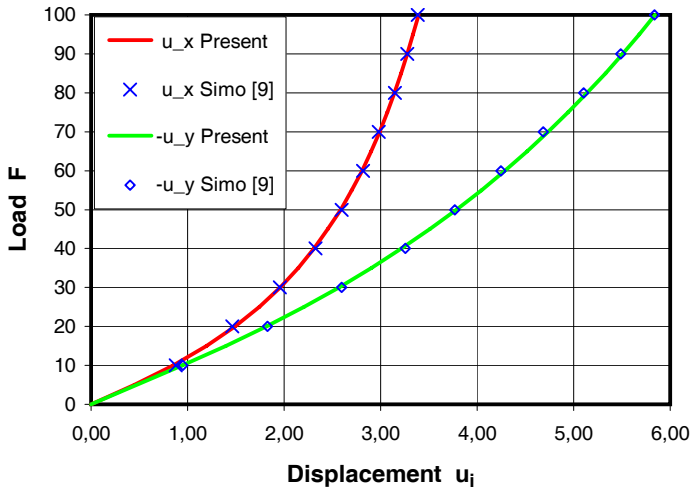

Iterat.	EAS-shell [17]	present element
1	5.6568542E+01	5.6568542E+01
2	2.7885600E+06	2.8374888E+06
3	4.6613004E+05	3.3241348E+05
4	1.9427725E+05	2.4512080E+04
5	6.7170299E+04	2.8536896E+02
6	2.6142653E+04	4.5611620E-02
7	1.3555091E+04	1.5785771E-08
8	3.5529025E+03	
9	5.5833012E+03	
10	9.2807935E+02	
11	4.6902795E+03	
12	2.0239489E+02	
13	2.2367207E+03	
14	1.4962903E+01	
15	2.2588811E+03	
16	9.1847138E-01	
17	1.4030970E+01	
18	5.8607442E-04	
19	9.5610236E-06	

Figure 6: Load deflection diagram and comparison of iteration behaviour

4.4 L–shaped beam

In the next geometrical nonlinear example we investigate the post–critical behaviour of a clamped L–shaped beam, origionally proposed in [39], see Fig. 7. The geometrical data are: length $l = 240\ mm$, width $b = 30\ mm$ and thickness $h = 0.6\ mm$. The elastic constants are $E = 71240\ N/mm^2$ and $\nu = 0.31$. A buckling load of $P_c = 1.09$ has been determined in [39] using beam elements, see also [40]. However with a width to height ratio 1/50 the beam is rather a thin plate. Thus a discretisation with shell elements leads to slightly different results. The post–critical path can be reached for the perfect structure using a branch switching procedure or with the introduction of imperfections, for example a small perturbation load $P_3 = P/1000$ in thickness direction. Nonlinear buckling loads are presented in Tab. 3 for different FE–meshes. Here the loading position has a significant influence on the buckling load. The complete load–deflection curve is computed using an arc–length scheme on the 68 element mesh. It is nearly identical to results obtained with the EAS–shell [17] and is depicted in Fig. 8. The robustness of the present element in comparison to the element [17] is demonstrated by the equilibrium iteration for a large step (from $u_3 = 19.540\ mm$ to $u_3 = 35.614\ mm$), see Fig. 8. Furthermore the initial mesh and the deformed mesh (for a displacement $u_3 = 56.1\ mm$) are plotted in Fig. 7.

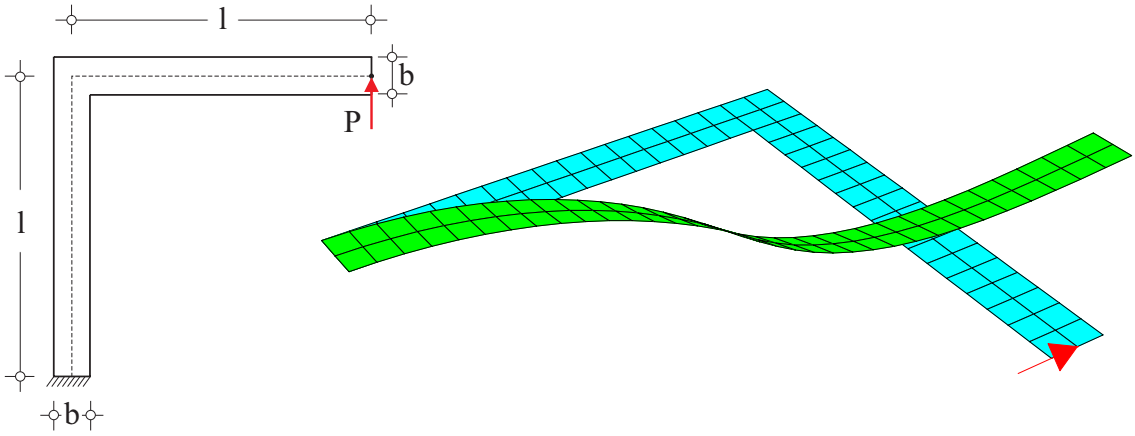

Figure 7: Geometry, initial and deformed mesh at displacement $u_3 = 56.1$ mm

Table 3: Nonlinear buckling loads

mesh for one leg	elements	Simo et al. [9]	EAS-shell [17]	present		
			center	bottom	center	top
16×2	68	1.137	1.200	1.137	1.198	1.258
32×4	272		1.191	1.128	1.190	1.248
64×8	1088		1.186	1.125	1.186	1.244
'converged solution' [9]		1.128				

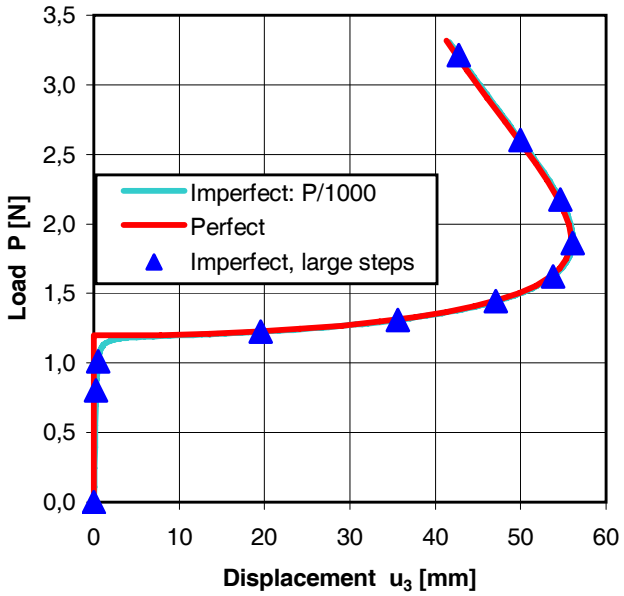

Iterat.	EAS-shell [17]	present
1	9.3256220E+04	1.0269311E+05
2	2.8840619E+03	1.8419593E+03
3	1.8272735E+03	9.2095431E+02
4	9.8608350E+01	3.1491938E-01
5	1.4371684E+02	7.2982781E-02
6	1.9857848E+01	3.6491332E-02
7	5.2637887E+01	7.7310783E-07
8	1.4549719E+01	4.3099687E-09
9	5.5153927E+01	
10	1.9751270E+00	
11	6.6634091E+01	
12	4.6571811E-02	
13	2.5106273E+00	
14	3.7558851E-05	
15	3.7154558E-06	
16	5.8605419E-09	

Figure 8: Load deflection diagram and iteration behaviour of residuum

4.5 Channel–section beam

A channel–section beam clamped at one end and subjected to a tip force at the free end is investigated next, see Fig. 9. In a first calculation we assume linear elastic behaviour and in a second step the elasto–plastic material model accoording to appendix E with constants according to Fig. 9. The developed shell model is compared with an EAS–shell model, [17]. The discretization is performed with 360 four–noded shell elements. The shell discretization consists of 36 elements along the length direction, 6 elements along the web and 2 elements for each flange. In the elastic case we apply load control whereas for the elasto–plastic case an arc–length scheme with displacement control is used. We calculate the structural behaviour up to a tip displacement of $w = 250$ cm and then unload the structure. The results for both models agree very good in the total range of the computed load deflection curves, see Figs. 10–11. This holds for elastic as well as for inelastic material behaviour. Fig. 12 shows a plot of the von Mises stresses for the ultimate state and the unloaded state. Similar results can be achieved using an elasto–plastic beam model, see [30]

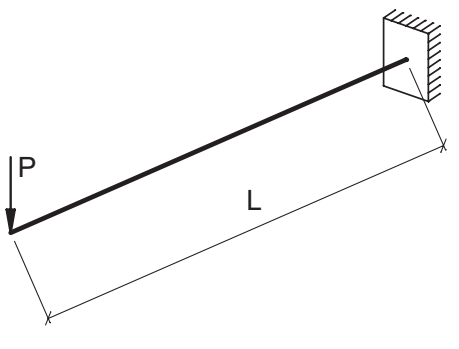

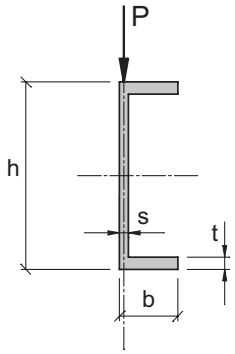

L	=	900	cm
h	=	30	cm
b	=	10	cm
s	=	1.0	cm
t	=	1.6	cm
E	=	21000	kN/cm^2
ν	=	0.3	
y_0	=	36	kN/cm^2
K	=	0	

Figure 9: Channel–section beam with geometrical and material data

The robustness of the iteration behaviour is decribed in the following. Large steps are possible for the present element for elastic as well as elasto–plastic material behaviour, see e.g. Figs.

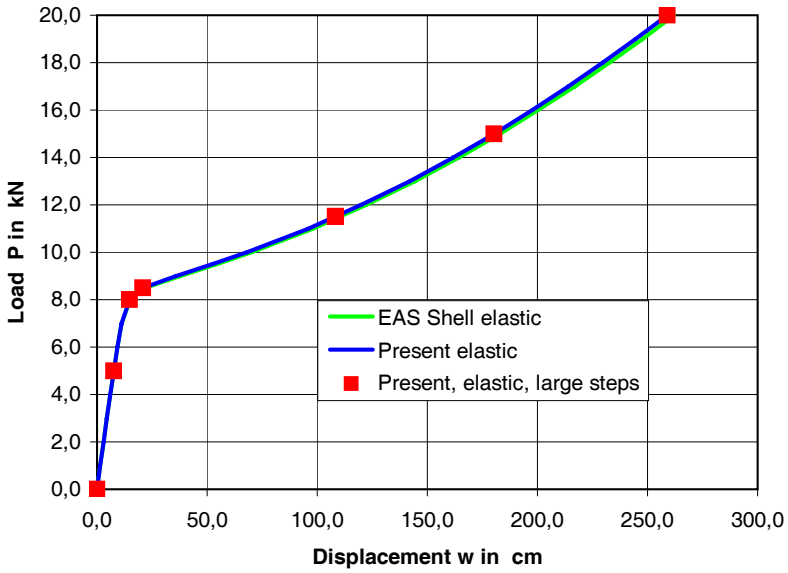

Figure 10: Load deflection curves of the channel–section beam: elastic material behaviour

10–11. The EAS–element with four enhanced parameters is much more sensitive and allows e.g. for the elasto–plastic case only displacement steps of $\Delta w \approx 1 - 3$ cm, whereas with the present element displacement steps of $\Delta w \approx 50 - 70$ cm are possible, see Fig. 11. The iteration behaviour of both element formulations is depicted for two steps in Tab. 4.

Table 4: Comparison of iteration behaviour in the elasto–plastic case

displacement step w: 50 → 53 cm		
Iterat.	EAS-shell [17]	present element
1	1.0000000E+00	1.0000000E+00
2	6.3761516E+03	5.5798017E+03
3	1.4983476E+02	2.8338326E+01
4	8.3009989E+01	5.0787877E-03
5	1.0505898E+01	3.4263339E-08
6	9.8385135E+00	
7	5.7130968E+00	
8	1.2059626E+00	
9	2.5993786E-01	
10	3.0121923E-03	
11	1.9727645E-05	
12	2.2762804E-08	

displacement step w: 50 → 120 cm		
Iterat.	EAS-shell [17]	present element
1	no convergence	1.0000000E+00
2		4.7604831E+06
3		1.5814845E+06
4		1.6610973E+05
5		1.2818501E+04
6		3.5064220E+01
7		1.6863763E-01
8		4.2263405E-06
9		1.9314382E-08
10		
11		
12		

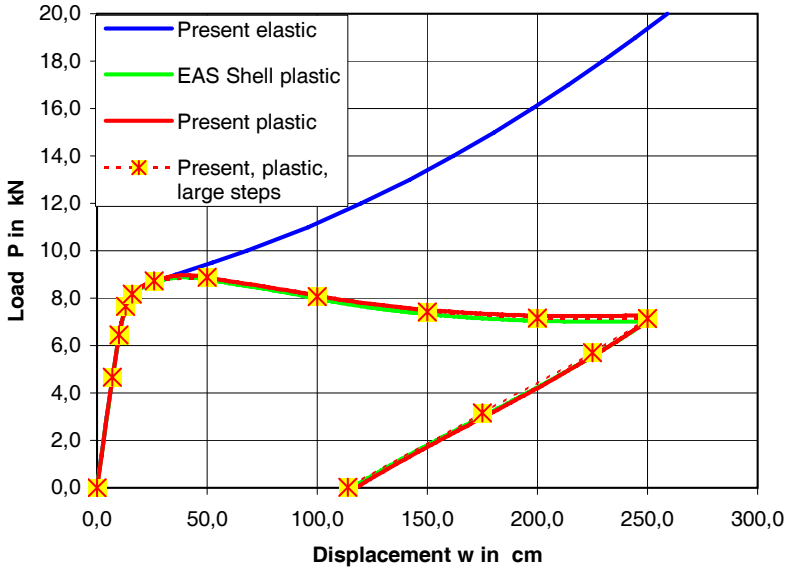

Figure 11: Load deflection curves of the channel–section beam: elasto–plastic material behaviour

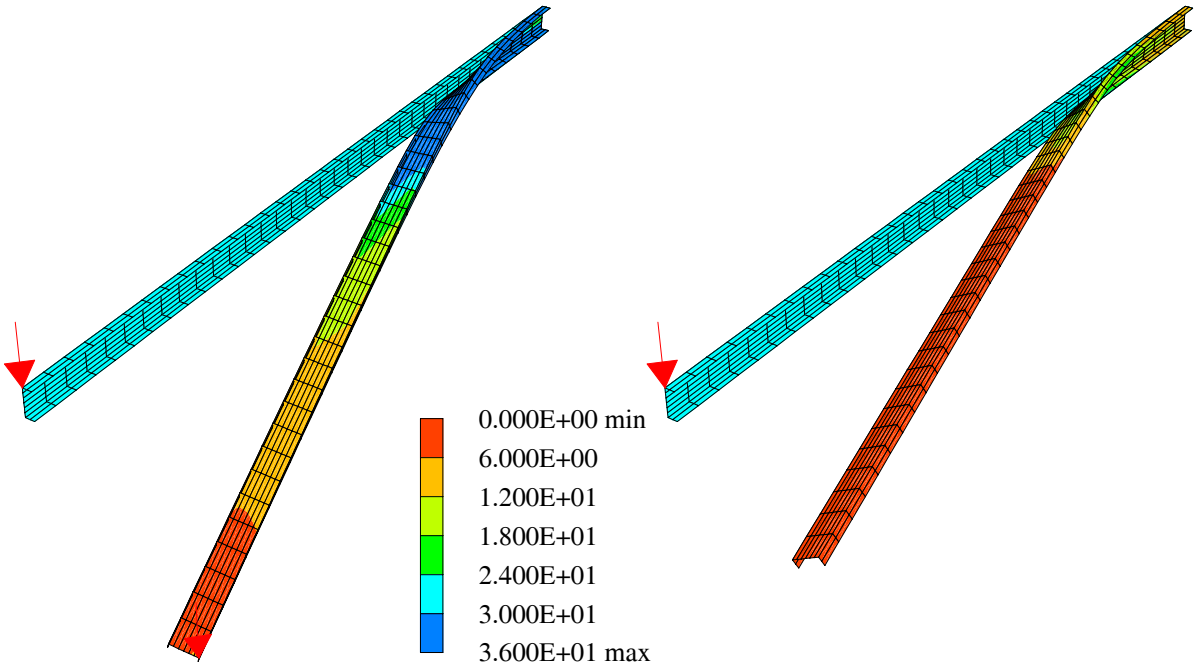

Figure 12: Von Mises stresses in kN/cm^2 for the ultimate state and unloaded state

4.6 Steel girder with holes

In the last example we discuss the stability behaviour of a beam with holes in a thin web subjected to a vertical load P at the center. Fig. 13 shows the ultimate buckling state in a similar experiment and the essential geometrical data. Experimental results are not available.

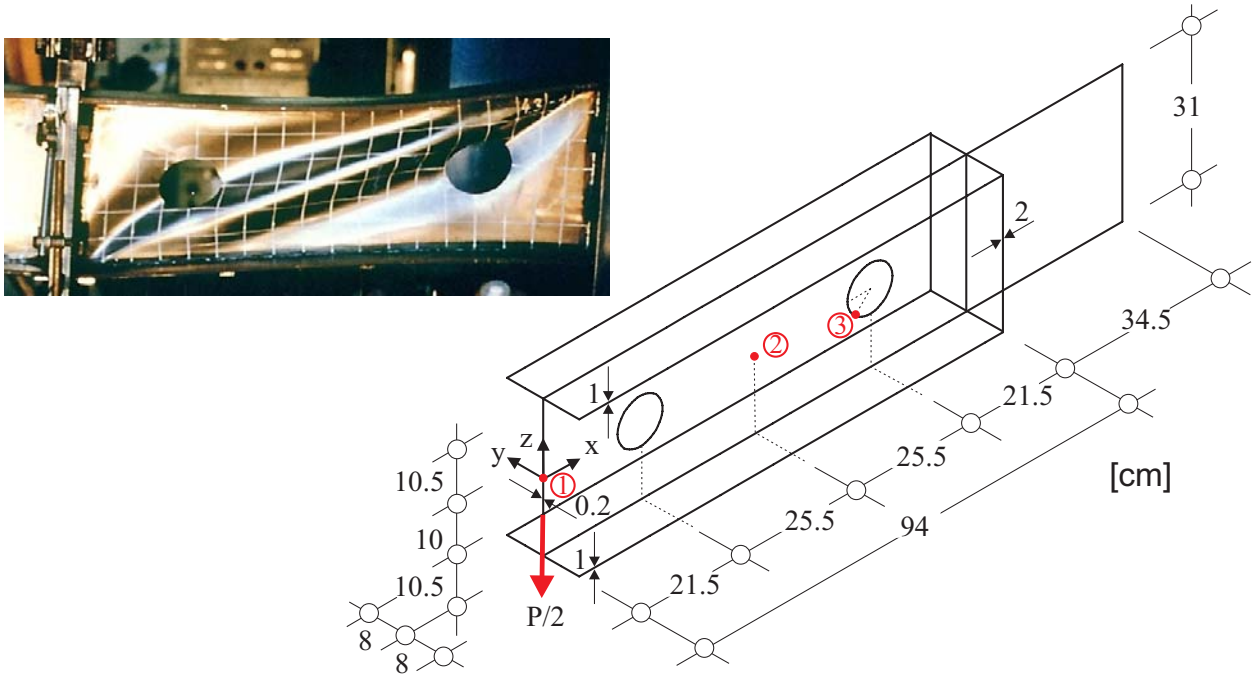

Figure 13: Steel girder with holes: a) similar experiment, b) geometrical data

A constant load distribution over the web is assumed. The web is modelled in the range ($94 < x < 128.5$ cm) as a rigid plate. The following boundary conditions are taken into account: symmetry conditions at x=0, fully clamped at x=128.5 cm. Furthermore no deflections in y-direction are permitted at x=y=0. $E = 21000\ kN/cm^2$ and $\nu = 0.3$ are chosen as elastic material properties. Within a pure elastic solution the load deflection curves for three selected points are depicted in Fig. 13. Here, an arc–length scheme and a branch switching procedure at the first buckling point have been used. Since the web is very thin the first buckling mode is governed by local buckles around the holes in the web, see Fig. 15. Again the developed element allows large load steps in the post–critical range.
In a second calculation we assume an ideal plastic material behaviour described by the model according to appendix E with a yield stress $y_0 = 36\,kN/cm^2$. Results for the associated load–deflection behaviour of the defined points are depicted in Fig. 16. Here the arc–length scheme is mandatory due to the decreasing load deflection curve. A similar deformation pattern is obtained. Since the web is very thin yielding occurs in large ranges starting from the holes, see Fig. 17, where the von Mises stresses are plotted with respect to the deformed mesh.

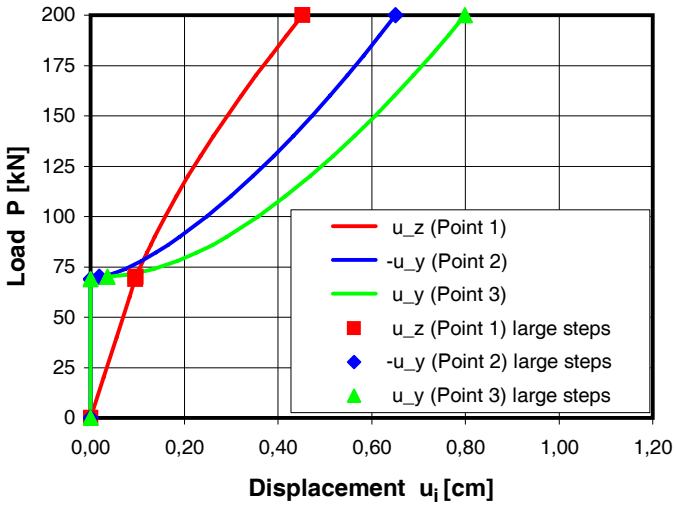

Figure 14: Load deflection curves in the elastic case

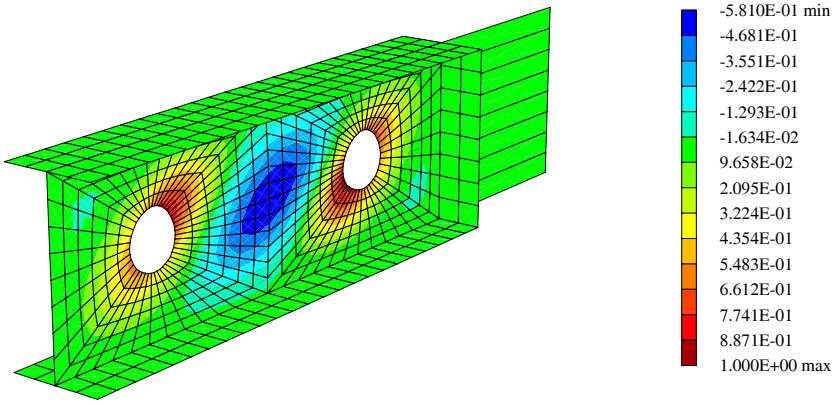

Figure 15: Displacement u_y of first buckling mode

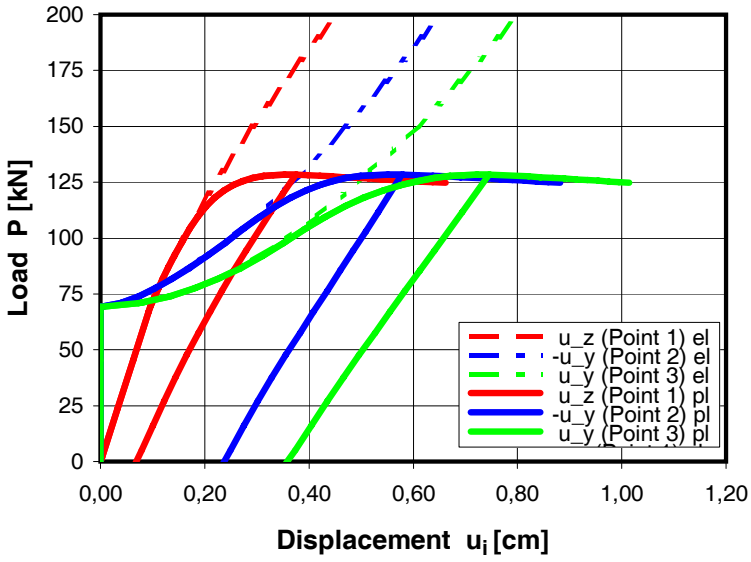

Figure 16: Load deflection curves in the elasto–plastic case

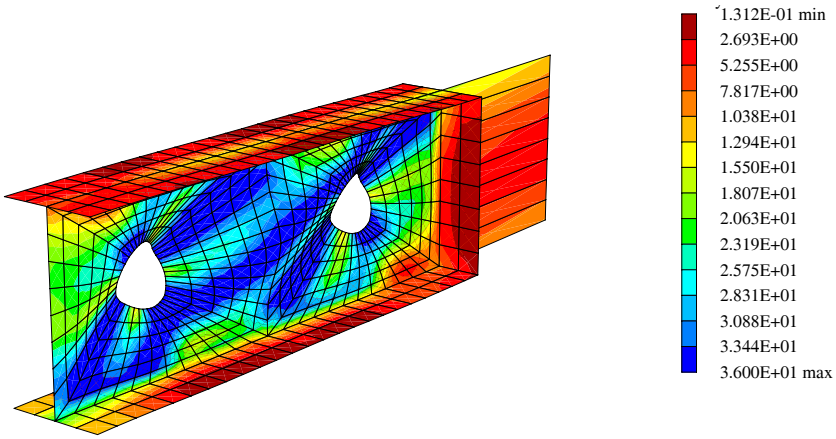

Figure 17: Von Mises stresses at ultimate load P=128 kN

5 Conclusions

An efficient quadrilateral shell element for the nonlinear analysis of thin structures is presented. Based on a Hu–Washizu variational functional appropriate interpolation functions for the independent mechanical fields are introduced. The developed mixed hybrid element allows very large load steps and requires essentially less equilibrium iterations in comparison to enhanced strain elements. This has been illustrated by several numerical examples which include bifurcation and post–buckling response and elasto–plastic material behaviour.

Appendix

A Second variation of the current director vector

The second variation of the current director vector reads according to [30]

$$
\begin{aligned}
\mathbf{h}_I \cdot \Delta\delta\mathbf{d}_I &= \delta\mathbf{w}_I \cdot \mathbf{M}_I\, \Delta\mathbf{w}_I \\
\mathbf{M}_I(\mathbf{h}_I) &= \tfrac{1}{2}(\mathbf{d}_I \otimes \mathbf{h}_I + \mathbf{h}_I \otimes \mathbf{d}_I) + \tfrac{1}{2}(\mathbf{t}_I \otimes \boldsymbol{\omega}_I + \boldsymbol{\omega}_I \otimes \mathbf{t}_I) + c_{10}\mathbf{1} \\
\mathbf{t}_I &= -c_3\, \mathbf{b}_I + (c_6 + c_2 c_9)\, (\mathbf{b}_I \cdot \boldsymbol{\omega}_I)\, \boldsymbol{\omega}_I \\
\mathbf{b}_I &= \mathbf{d}_I \times \mathbf{h}_I \\
c_2 &= \frac{\omega_I - \sin\omega_I}{\omega_I^3} \\
c_3 &= \frac{\omega_I \sin\omega_I + 2\cos\omega_I - 2}{\omega_I^2\,(\cos\omega_I - 1)} \\
c_6 &= \frac{c_3 - c_2}{\omega_I^2} \\
c_9 &= -\tfrac{1}{4} + c_3 - \tfrac{1}{4}\omega_I^2 c_3^2 \\
c_{10} &= c_2(1 - c_9\,\omega_I^2)\, (\mathbf{b}_I \cdot \boldsymbol{\omega}_I) - (\mathbf{d}_I \cdot \mathbf{h}_I)
\end{aligned}
\tag{49}
$$

where $\mathbf{h}_I \in \boldsymbol{R}^3$ denotes an arbitrary vector .

B Remarks on patch test and stability

Assuming infinitesimal deformations $\delta\mathbf{v}_e$ $e = 1, 2..., numel$ we examine conditions to fulfil the patch test and stability conditions for the discrete problem based on the presented mixed formulation. The described FE–method can be interpreted as a $\bar{\boldsymbol{B}}-$ approach.

B.1 The patch test

Introduce

$$\bar{\mathbf{B}} := \mathbf{N}_\varepsilon \, \mathbf{F}^{T-1} \, \mathbf{G} \tag{50}$$

the material part of the element stiffness matrix can be reformulated as follows

$$\mathbf{k}_m = \mathbf{G}^T \, \hat{\mathbf{H}} \, \mathbf{G} = \int\limits_{(\Omega_e)} \bar{\mathbf{B}}^T \, \mathbf{C} \, \bar{\mathbf{B}} \, dA \,. \tag{51}$$

Now consider an element displacement vector $\delta\mathbf{v}$, such that

$$\mathbf{B} \, \delta\mathbf{v} \equiv \text{constant} \tag{52}$$

for each element and formulate

$$\bar{\mathbf{B}} \, \delta\mathbf{v} = \mathbf{N}_\varepsilon \, \mathbf{F}^{T-1} \, \mathbf{G} \, \delta\mathbf{v} = \left[\mathbf{1}, \tilde{\mathbf{N}}_\varepsilon\right] \begin{bmatrix} 1/A_e \, \mathbf{1} & \mathbf{0} \\ \mathbf{0} & \mathbf{f}^{T-1} \end{bmatrix} \begin{bmatrix} \int\limits_{(\Omega_e)} \mathbf{B} \, \delta\mathbf{v} \, dA \\ \int\limits_{(\Omega_e)} \tilde{\mathbf{N}}_\sigma^T \, \mathbf{B} \, \delta\mathbf{v} \, dA \end{bmatrix} \tag{53}$$

which yields

$$\bar{\mathbf{B}} \, \delta\mathbf{v} = \boldsymbol{\varepsilon}^0 \equiv \text{constant} \tag{54}$$

if the following two conditions hold:

(i) $\frac{1}{A_e} \int_{(\Omega_e)} \mathbf{B} \, \delta\mathbf{v} \, dA = \mathbf{B}(\xi = \eta = 0) \, \delta\mathbf{v} = \boldsymbol{\varepsilon}^0$. This is fulfilled for the shear part with assumed strains, but not with the standard bilinear finite element interpolation of the displacement field along with $(5)_3$. In this context we refer to the investigations for a linear plate [33].

(ii) $\int_{(\Omega_e)} \tilde{\mathbf{N}}_\sigma^T \, dA = \mathbf{0}$, which is the case for the present interpolation.

Thus $\boldsymbol{\varepsilon}^0 \equiv$ constant yields with $\mathbf{C} =$ constant for an arbitrary patch of elements to a constant stress state.

B.2 Stability of the discrete problem

Here the numerical stability of the presented mixed hybrid shell element with 20 nodal degrees of freedom based on the Hu–Washizu functional is discussed. We assume that $\mathbf{C}$ is positive definite and that the geometric contribution to the tangential stiffness does not introduce instabilities. We denote by ker[$\mathbf{B}$] the null space of $\mathbf{B}$. Recall that ker[$\mathbf{B}$] consists all nodal infinitesimal rigid body motions, i.e. a vector $\delta\mathbf{v}^R$ in ker[$\mathbf{B}$] satisfies

$$\mathbf{B} \, \delta\mathbf{v}^R = \mathbf{0} \quad \Leftrightarrow \quad \delta\mathbf{v}^R = \text{nodal rigid body motion} \tag{55}$$

and thus from (50)

$$\bar{\mathbf{B}}\,\delta\mathbf{v}^R = \mathbf{N}_\varepsilon\,\mathbf{F}^{T-1}\int\limits_{\Omega_e}\mathbf{N}_\sigma^T\,\mathbf{B}\,\delta\mathbf{v}^R\,dA = \mathbf{0}\,. \tag{56}$$

Thus we conclude for a unique solution that the material tangent matrix must be at least positive semidefinite

$$\delta\mathbf{v}^T\,\mathbf{k}_m\delta\mathbf{v}\;\geq 0 \qquad \forall\;\delta\mathbf{v}\,, \tag{57}$$

with $\mathbf{k}_m$ according to (51). The equal sign holds for the admissible rigid body motions. For the present quadrilateral element with $n_u = 20$ degrees of freedom and $n_r = 6$ rigid body modes eq. (57) imposes the following restrictions on $\mathbf{N}_\sigma$ and $\mathbf{N}_\epsilon$:

(i) The columns of $\mathbf{N}_\sigma$ and $\mathbf{N}_\varepsilon$ are linear independent, or equivalent $\mathbf{F}$ is positive definite.

(ii) The number of stress and strain parameters n_ε must fulfill $n_\varepsilon \geq n_u - n_r = 14$.

(iii) In view of (55)and (56) the constraint $\ker[\bar{\mathbf{B}}] = \ker[\mathbf{B}]$ yields the requirement that the rank of matrix $\mathbf{G}$ must be equal to n_ε.

The conditions are fulfilled for the present element. It possesses with 6 zero eigenvalues which correspond to the rigid motions the correct rank.

C Numerical integration of the stress resultants

The relation between the strains at a layer point with coordinate ξ^3 and the shell strains (4) is rewritten in matrix notation

$$\begin{bmatrix} E_{11}\\ E_{22}\\ 2E_{12}\\ 2E_{13}\\ 2E_{23}\end{bmatrix} = \begin{bmatrix} 1&0&0&\xi^3&0&0&0&0\\ 0&1&0&0&\xi^3&0&0&0\\ 0&0&1&0&0&\xi^3&0&0\\ 0&0&0&0&0&0&1&0\\ 0&0&0&0&0&0&0&1\end{bmatrix}\begin{bmatrix}\varepsilon_{11}\\ \varepsilon_{22}\\ 2\varepsilon_{12}\\ \kappa_{11}\\ \kappa_{22}\\ 2\kappa_{12}\\ \gamma_1\\ \gamma_2\end{bmatrix} \tag{58}$$

$$\mathbf{E}_m = \mathbf{A}\,\boldsymbol{\varepsilon}$$

The kinematic shell model assumes inextensibility in thickness direction. Thus the plane stress condition has to be enforced which then yields the thickness strains, see e.g. [41]. Therefore the reduced vector $\mathbf{S}^m = [S^{11}, S^{22}, S^{12}, S^{13}, S^{23}]^T$ with components of the Second Piola–Kirchhoff stresses is introduced.
Inserting (58) in the internal virtual work expression of the body $\delta W^i = \int_\Omega \int_{(\xi^3)} \delta\mathbf{E}_m^T\mathbf{S}^m\,\bar{\mu}\,d\xi^3 d\,\Omega$ yields the vector of the stress resultants

$$\partial_{\boldsymbol{\varepsilon}} W = \int\limits_{(-h/2)}^{(h/2)}\mathbf{A}^T\mathbf{S}^m\,\bar{\mu}\;d\xi^3 \tag{59}$$

where $\bar{\mu}$ denotes the determinant of the so–called shifter tensor.

The plane stress condition $S^{33}(E_{33}) = 0$ is iteratively enforced. For this purpose the increment of the Second Piola–Kirchhoff stress tensor is written as follows

$$\begin{aligned} \begin{bmatrix} \mathrm{d}\mathbf{S}^m \\ \mathrm{d}S^{33} \end{bmatrix} &= \begin{bmatrix} \mathbf{C}^{mm} & \mathbf{C}^{m3} \\ \mathbf{C}^{3m} & C^{33} \end{bmatrix} \begin{bmatrix} \mathrm{d}\mathbf{E}_m \\ \mathrm{d}E_{33} \end{bmatrix} \\ \mathrm{d}\mathbf{S} &= \bar{\mathbf{C}}\,\mathrm{d}\mathbf{E} \end{aligned} \tag{60}$$

where $\bar{\mathbf{C}}$ denotes the linearized Second Piola–Kirchhoff stress tensor which is determined within a three–dimensional stress analysis at the considered layer point.
The Taylor series of the plane stress condition is aborted after the linear term and set to zero

$$S^{33}(E_{33}^{(i)} + \Delta E_{33}^{(i)}) = S^{33(i)} + \frac{\partial S^{33(i)}}{\partial E_{33}^{(i)}}\,\Delta E_{33}^{(i)} = 0 \qquad \text{with} \qquad \frac{\partial S^{33(i)}}{\partial E_{33}^{(i)}} = C^{33(i)} \tag{61}$$

and the solution yields the update formula

$$E_{33}^{(i+1)} = E_{33}^{(i)} - \frac{S^{33(i)}}{C^{33(i)}} \tag{62}$$

where i denotes the iteration number. Thus the nonlinear scalar equation $S^{33}(E_{33}) = 0$ is iteratively solved for the unknown thickness strains using Newton´s scheme. One obtains the stress vector $\mathbf{S}^m$ and the tangent matrix $\bar{\mathbf{C}}$ with submatrices according to (60). For constitutive equations with a linear relation between $\mathbf{S}$ and $\mathbf{E}$ only one iteration step is necessary. This is e.g. the case for isotropy when using the so–called St.Venant Kirchhoff law. Finally the linearization of the stress resultants (59) considering the kinematic equation (58) yields

$$\mathbf{C} = \frac{\partial^2 W}{\partial \boldsymbol{\varepsilon}^2} = \int_{(-h/2)}^{(h/2)} \mathbf{A}^T\,\frac{\partial \mathbf{S}^m}{\partial \mathbf{E}_m}\,\frac{\partial \mathbf{E}_m}{\partial \boldsymbol{\varepsilon}}\,\bar{\mu}\;d\xi^3 = \int_{(-h/2)}^{(h/2)} \mathbf{A}^T\,\tilde{\mathbf{C}}^{mm}\,\mathbf{A}\,\bar{\mu}\;d\xi^3 \tag{63}$$

where $\tilde{\mathbf{C}}^{mm} = \mathbf{C}^{mm} - \mathbf{C}^{m3}\,(C^{33})^{-1}\,\mathbf{C}^{3m}$ is obtained by static condensation of $\mathrm{d}E_{33}$ in (60).
Summarizing the algorithm provides an interface to arbitrary nonlinear three–dimensional material laws. It requires the computation of $\mathbf{S}$ and $\bar{\mathbf{C}}$ which is a standard output of any nonlinear three–dimensional stress analysis. It is important to note that in the Hu–Washizu functional (19) the independent strains $\boldsymbol{\varepsilon}$ enter into the constitutive model, and thus in (58). The thickness integration in (59) and (63) is performed numerically by summation over layers and with two Gauss integration points for each layer. The numerical computations show that four layers are sufficient when considering inelastic material behaviour. Since we use an orthogonal basis system at the element center $\bar{\mu} = 1$ holds only at the center. The numerical tests however show that $\bar{\mu} = 1$ can be set for the whole element and convergence against the correct solution is given. In case of a constant matrix $\tilde{\mathbf{C}}^{mm}$, or a constant matrix for each layer in laminated shells, an analytical thickness integration is possible.

D Analytical integration of some matrices

The area element of the shell middle surface $d\,A = |\mathbf{X}_{,\xi} \times \mathbf{X}_{,\eta}|\; d\xi d\eta$ can be approximated in case of arbitrary warped elements by

$$|\mathbf{X}_{,\xi} \times \mathbf{X}_{,\eta}| \approx \det \mathbf{J} \tag{64}$$

with $\mathbf{J}$ according to (14)

$$\begin{aligned} \det \mathbf{J} &= j_0 + \xi\, j_1 + \eta\, j_2 \\ j_0 &= (\mathbf{G}^0_\xi \cdot \mathbf{t}_1)(\mathbf{G}^0_\eta \cdot \mathbf{t}_2) - (\mathbf{G}^0_\eta \cdot \mathbf{t}_1)(\mathbf{G}^0_\xi \cdot \mathbf{t}_2) = |\mathbf{G}^0_\xi \times \mathbf{G}^0_\eta| \\ j_1 &= (\mathbf{G}^0_\xi \cdot \mathbf{t}_1)(\mathbf{G}^1 \cdot \mathbf{t}_2) - (\mathbf{G}^1 \cdot \mathbf{t}_1)(\mathbf{G}^0_\xi \cdot \mathbf{t}_2) = \mathbf{t}_3 \cdot (\mathbf{G}^0_\xi \times \mathbf{G}^1) \\ j_2 &= (\mathbf{G}^1 \cdot \mathbf{t}_1)(\mathbf{G}^0_\eta \cdot \mathbf{t}_2) - (\mathbf{G}^0_\eta \cdot \mathbf{t}_1)(\mathbf{G}^1 \cdot \mathbf{t}_2) = \mathbf{t}_3 \cdot (\mathbf{G}^1 \times \mathbf{G}^0_\eta)\,. \end{aligned} \tag{65}$$

The reason for the approximation is the constant element basis system $\mathbf{t}_i$ in (14). Using (65) the integration of the constants $\bar\xi$ and $\bar\eta$ yields

$$\bar\xi = \frac{1}{A_e}\int_{(\Omega_e)} \xi\, dA = \frac{1}{3}\frac{j_1}{j_0} \qquad\qquad \bar\eta = \frac{1}{A_e}\int_{(\Omega_e)} \eta\, dA = \frac{1}{3}\frac{j_2}{j_0} \tag{66}$$

with the element area $A_e = 4 j_0$.
With these results the matrix $\mathbf{F}$ can be integrated analytically, since only polynomials of the coordinates ξ and η are involved. Due to the introduced constants $\bar\xi$ and $\bar\eta$ one obtains a decoupled matrix

$$\mathbf{F} = \begin{bmatrix} A_e\,\mathbf{1}_8 & \mathbf{0} \\ \mathbf{0} & \mathbf{f}_{(6\times6)} \end{bmatrix} \qquad \text{with} \qquad \mathbf{f}_{(6\times6)} = \begin{bmatrix} \mathbf{f}^m & \mathbf{0} & \mathbf{0} \\ \mathbf{0} & \mathbf{f}^b & \mathbf{0} \\ \mathbf{0} & \mathbf{0} & \mathbf{f}^s \end{bmatrix}. \tag{67}$$

The components of the symmetric sub-matrices $\mathbf{f}^m = \mathbf{f}^b$ and $\mathbf{f}^s$ are specified

$$\begin{aligned} \mathbf{f}^m &= \frac{A_e}{3}\begin{bmatrix} \hat f_{11}\,(J^0_{11}J^0_{11} + J^0_{12}J^0_{12})^2 & \hat f_{12}\,(J^0_{11}\,J^0_{21} + J^0_{22}J^0_{12})^2 \\ \hat f_{12}\,(J^0_{11}\,J^0_{21} + J^0_{22}J^0_{12})^2 & \hat f_{22}\,(J^0_{21}J^0_{21} + J^0_{22}J^0_{22})^2 \end{bmatrix} \\ \mathbf{f}^s &= \frac{A_e}{3}\begin{bmatrix} \hat f_{11}\,(J^0_{11}J^0_{11} + J^0_{12}J^0_{12}) & \hat f_{12}\,(J^0_{11}\,J^0_{21} + J^0_{22}J^0_{12}) \\ \hat f_{12}\,(J^0_{11}\,J^0_{21} + J^0_{22}J^0_{12}) & \hat f_{22}\,(J^0_{21}J^0_{21} + J^0_{22}J^0_{22}) \end{bmatrix} \end{aligned} \tag{68}$$

with $\hat f_{11} = 1 - 3\,\bar\eta^2$, $\hat f_{22} = 1 - 3\,\bar\xi^2$ and $\hat f_{12} = -3\,\bar\xi\,\bar\eta$. $\mathbf{F}$ can be constructed completely diagonal if all columns of (38) and (40) are orthogonal. For linear elastic material behaviour with $\mathbf{C} = \text{diag}\,[\mathbf{C}^m, \frac{h^2}{12}\mathbf{C}^m, \frac{5}{6}Gh\,\mathbf{1}] = \text{constant}$ the matrix $\mathbf{H}$ obtains a structure comparable to $\mathbf{F}$

$$\mathbf{H} = \begin{bmatrix} A_e\,\mathbf{C} & \mathbf{0} \\ \mathbf{0} & \mathbf{h}_{(6\times6)} \end{bmatrix} \quad \text{with} \quad \mathbf{h}_{(6\times6)} = \begin{bmatrix} \mathbf{h}^m & \mathbf{0} & \mathbf{0} \\ \mathbf{0} & \mathbf{h}^b & \mathbf{0} \\ \mathbf{0} & \mathbf{0} & \mathbf{h}^s \end{bmatrix} \quad \begin{aligned} \mathbf{h}^m &= \textstyle\int_{\Omega_e} \mathbf{N}^{mT}_\varepsilon\, \mathbf{C}^m\, \mathbf{N}^m_\varepsilon\; dA \\ \mathbf{h}^b &= \tfrac{h^2}{12}\,\mathbf{h}^m \\ \mathbf{h}^s &= \tfrac{5}{6}\,Gh\,\mathbf{f}^s \end{aligned}, \tag{69}$$

where $\mathbf{h}^m$ can also be integrated analytically.

E J_2-plasticity model for small strains

The applied plasticity model is restricted to small strains, where the additive decomposition of the Green–Lagrangean strains in elastic an plastic parts is assumed. The strain energy is a quadratic function of the elastic strains. We use an associative flow rule and a J_2 yield criterion with linear isotropic hardening. The constitutive equations are summarized as follows:

$$
\begin{aligned}
&\text{kinematic assumption} && \mathbf{E} &&= \mathbf{E}_e + \mathbf{E}_p \\
&\text{elastic part of the free energy} && \psi(\mathbf{E}_e) &&= \tfrac{\lambda}{2}\,(\mathrm{tr}\mathbf{E}_e)^2 + G\,\mathrm{tr}(\mathbf{E}_e^2) \\
&\text{Second Piola–Kirchhoff stresses} && \mathbf{S} &&= \partial_{E_e}\psi \\
&\text{linear isotropic hardening} && y(e^p) &&= y_0 + K\,e_p \\
&\text{yield criterion} && \Phi &&= \sqrt{\tfrac{3}{2}}\,||\mathrm{dev}\,\mathbf{S}|| - y(e_p) \\
&\text{associative flow rule} && \dot{\mathbf{E}}_p &&= \gamma\,\partial_S\Phi \\
&\text{evolution of } e_p && \dot{e}_p &&= \sqrt{\tfrac{2}{3}}\;||\dot{\mathbf{E}}_p|| \\
&\text{loading unloading conditions} && \gamma \geq 0,\ \Phi \leq 0,\ && \gamma\,\Phi = 0
\end{aligned}
\tag{70}
$$

Here, the Lamé parameter λ is related to the elasticity constants by $\lambda = \frac{E\nu}{(1+\nu)(1-2\nu)}$, G denotes the shear modulus, y_0 the initial yield stress and K the plastic tangent modulus. The rate equations are integrated with a backward Euler algorithm. The stress tensor is linearized to obtain the consistent tangent matrix $\bar{\mathbf{C}}$ introduced in (60).

Remark:
The definition of the deviatoric part of the Second Piola–Kirchhoff stress tensor for finite strain kinematics is

$$
\mathrm{Dev}\,\mathbf{S} = \mathbf{S} - \frac{1}{3}[\mathbf{S} : \hat{\mathbf{C}}]\hat{\mathbf{C}}^{-1}\,. \tag{71}
$$

Since $\hat{\mathbf{C}} = (\mathbf{1} + 2\mathbf{E})$, then for small Green–Lagrangean strains (i.e. when $\|\mathbf{E}^2\| \ll \|\mathbf{E}\| \ll 1$) it follows that

$$
\mathrm{Dev}\,\mathbf{S} = \mathbf{S} - \frac{1}{3}[\mathbf{S} : \mathbf{1}] + \mathcal{O}(\|\mathbf{E}\|) = \mathrm{dev}\,\mathbf{S} + \mathcal{O}(\|\mathbf{E}\|)\,. \tag{72}
$$

Here $\mathcal{O}(\|\mathbf{E}\|)$ denotes the terms which tend to zero as $\|\mathbf{E}\|$ approaches zero. Thus, when strains are restricted to be small, an approximate definition of the deviatoric stress tensor may be employed. Therefore in problems where finite rotations may be present but strains are restricted to be small, the above constitutive Eqs. (70) describe the small strain von Mises elasto–plasticity model. In this context we refer to [42].

References

[1] Koiter WT. On the nonlinear theory of thin elastic shells. *Proc. Kon. Ned. Ak. Wet. B69* 1966; 1-54. 1

[2] Green AE, Naghdi PM. On the derivation of shell theories by direct approach. *J. Appl. Mech.* 1974; **41**: 173–176. 1

[3] Ahmad S, Irons BM, Zienkiewicz OC. Analysis of thick and thin shell structures by curved finite elements. *Int. J. Num. Meth. Engng.* 1970; **2**: 419–451. 1

[4] Büchter N, Ramm E. Shell theory versus degeneration–A comparison in large rotation finite element analysis. *Int. J. Num. Meth. Engng.* 1992; **34**: 39–59. 1

[5] Reissner E. The effect of transverse shear deformation on the bending of elastic plates. *J. Appl. Mech.* 1945; **12**: 69–76. 1

[6] Mindlin RD. Influence of rotatory inertia and shear flexural motions of isotropic elastic plates. *J. Appl. Mech.* 1951; **18**: 31–38. 1

[7] Liu WK, Law SE, Lam D , Belytschko T. Resultant–stress degenerated shell element. *Comp. Meth. Appl. Mech. Engng.* 1986; **55**: 261–300. 1

[8] Stanley GM, Park KC, Hughes TJR. Continuum–Based Resultant Shell Elements. in: *Finite Element Methods for Plate and Shell Structures 1: Element Technology.* eds. TJR Hughes and E Hinton, Pineridge Press: Swansea, 1986. 1

[9] Simo JC, Rifai MS, Fox DD. On a stress resultant geometrically exact shell model. Part III: Computational aspects of the nonlinear theory. *Comp. Meth. Appl. Mech. Engng.* 1990; **79**: 21–70. 1, 4.3, 3

[10] Zienkiewicz OC, Taylor RL, Too J. Reduced integration techniques in general analysis of plates and shells. *Int. J. Num. Meth. Engng.* 1971; **3**: 275–290. 1

[11] Belytschko T, Tsay C-S. A stabilization procedure for the quadrilateral plate element with one–point quadrature. *Int. J. Num. Meth. Engng.* 1983; **19**: 405–419. 1

[12] Belytschko T, Lin JI, Tsay CS. Explicit algorithms for the nonlinear dynamics of shells. *Comp. Meth. Appl. Mech. Engrg.* 1984; **42**: 225–251. 1

[13] Vu-Quoc L, Mora JA. A Class of Simple and Efficient Degenerated Shell Elements–Analysis of Global Spurious-Mode Filtering. *Comp. Meth. Appl. Mech. Engng.* 1989; **74**: 117–175. 1

[14] Belytschko T, Leviathan I. Physical stabilization of the 4–node shell element with one point quadrature. *Comp. Meth. Appl. Mech. Engrg.* 1994; **113**: 321–350. 1

[15] Simo JC, Rifai MS. A class of mixed assumed strain methods and the method of incompatible modes. *Int. J. Num. Meth. Eng.* 1990; **29**: 1595–1638. 1

[16] Betsch P, Gruttmann F, Stein, E. A 4–Node Finite Shell Element for the Implementation of General Hyperelastic 3D–Elasticity at Finite Strains. *Comp. Meth. Appl. Mech. Eng.* 1996; **130**: 57–79. 1

[17] Sauer R: Eine einheitliche Finite–Element–Formulierung für Stab– und Schalentragwerke mit endlichen Rotationen. Bericht 4 (1998), Institut für Baustatik, Universität Karlsruhe (TH). 1, 1, 2, 4.3, 4.3, 4.4, 3, 4.4, 4.5, 4

[18] Klinkel S, Gruttmann F, Wagner W. A continuum based three-dimensional shell element for laminated structures. *Comput. & Struct.* 1999; **71**: 43–62. 1

[19] Vu-Quoc L, Tan XG. Optimal solid shells for non-linear analyses of multilayer composites. I. Statics. *Comp. Meth. Appl. Mech. Engng.* 2003; **192**: 975–1016. 1, 4.1

[20] Piltner R, Taylor RL. A systematic construction of B-bar functions for linear and non-linear mixed-enhanced finite elements for plane elasticity problems. *Int. J. Num. Meth. Eng.* 1999; **44**: 615–639. 1

[21] MacNeal RH. A simple quadrilateral shell element. *Comput. Struct.* 1978; **8**: 175–183. 1

[22] Hughes TJR, Tezduyar TE. Finite elements based upon Mindlin plate theory, with particular reference to the 4–node bilinear isoparametric element. *J. Appl. Mech.* 1981; **48**: 587–595. 1

[23] Dvorkin E, Bathe KJ. A continuum mechanics based four node shell element for general nonlinear analysis. *Engineering Computations* 1984; **1**: 77–88. 1, 3.2

[24] Bathe KJ, Dvorkin E. A 4–Node Plate bending element based on Mindlin/Reissner theory and a mixed interpolation. *Int. J. Num. Meth. Engng.* 1985; **21** 367–383. 1

[25] Gruttmann F, Wagner W, Wriggers P. A Nonlinear Quadrilateral Shell Element with Drilling Degrees of Freedom. *Arch. Appl. Mech.* 1992; **62**: 474–486. 1

[26] Hughes TJR. *The Finite Element Method, Linear static and Dynamic Finite Element Analysis*. Prentice–Hall, Inc., Englewood Cliffs: New Jersey, 1987. 3.1

[27] Taylor RL, Simo JC, Zienkiewicz OC, Chan ACH. The patch test - A condition for assessing FEM convergence. *Int. J. Num. Meth. Engng.* 1986; **22**: 39–62. 3.2

[28] Hughes TJR, Liu WK. Nonlinear finite element analysis of shells: Part I. Threedimensional shells. *Comp. Meth. Appl. Mech. Engrg.* 1981; **26**: 331–362. 3.2

[29] Simo JC. On a stress resultant geometrically exact shell model. Part VII: Shell intersections with 5/6-DOF finite element formulations. *Comp. Meth. Appl. Mech. Engrg.* 1993; **108** 319–339. 3.2

[30] Gruttmann F, Sauer R, Wagner W. Theory and Numerics of Three–Dimensional Beams with Elastoplastic Material Behaviour. *Int. J. Num. Meth. Engng.* 2000; **48**: 1675–1702. 3.2, 3.3, 4.5, 5

[31] Simo JC, Fox DD, Rifai M.S. On a stress resultant geometrically exact shell model. Part II: The linear theory; Computational aspects. *Comp. Meth. Appl. Mech. Engrg.* 1989; **73**: 53–92. 3.4, 1, 2

[32] Pian THH, Sumihara K. Rational approach for assumed stress finite elements. *Int. J. Num. Meth. Eng.* 1984; **20**: 1685-1695. 3.4

[33] Gruttmann F, Wagner W. A stabilized one–point integrated quadrilateral Reissner–Mindlin plate element. *Int. J. Num. Meth. Engng.* 2004; **61**: 2273-2295. 3.4, B.1

[34] Gruttmann F, Wagner W. A linear quadrilateral shell element with fast stiffness computation. *Comp. Meth. Appl. Mech. Eng.* in press 2005. 3.5, 4.2, 1, 2

[35] Zienkiewicz OC, Taylor RL. *The Finite Element Method*, Vol.1–3. 5. ed., Butterworth-Heinemann: Oxford, 2000. 4

[36] MacNeal RH., Harder RL. A proposed standard set of problems to test finite element accuracy. *Finite Elements in Analysis and Design* 1985; **1**: 3–20. 4.1, 4.2

[37] Jetteur P. Improvement of the quadrilateral Jet shell element for a particular class of shell problems. IREM Internal Report 87/1, Ecole Polytechnique Fédérale de Lausanne, 1987. 4.2

[38] Taylor RL. Finite element analysis of linear shell problems. in: J.R. Whiteman (Ed), *The Mathematics of Finite Elements and Applications VI, (MAFELAP 1987)*. Academic Press: London, 1988: 191–204. 4.2, 1, 2

[39] Argyris JH et al. Finite element method – the natural approach. *Comp. Meth. Appl. Mech. Engng.* 1979; **17/18**: 1–106. 4.4

[40] Simo JC, Vu-Quoc L. Three–dimensional finite strain rod model. Part II: Computational aspects. *Comp. Meth. Appl. Mech. Engng.* 1986; **58**: 79–116. 4.4

[41] Klinkel S, Govindjee S. Using finite strain 3D-material models in beam and shell elements. *Engineering Computations* 2002; **19**(8): 902–921. C

[42] Brank B, Perić D, Damjanić F. On large deformations of thin elasto-plastic shells: implementation of a finite rotation model for quadrilateral shell element *Int. J. Num. Meth. Engng.* 1997; **40**: 689–726. E